Study of the optimal location of wing sensors using model-order reduction

REPORT

Author: Belmonte Lauroba, Marc

Director: Hernández Ortega, Joaquín Alberto

Co-director: Cante Teran, Juan Carlos

Bachelor's Degree in Aerospace Technology Engineering

June 22nd, 2016

UNIVERSITAT POLITÈCNICA DE CATALUNYA
BARCELONATECH
Escola Superior d'Enginyeries Industrial,
Aeroespacial i Audiovisual de Terrassa

Index

List of Figures

List of Tables

1. Aim

The overall goal of this work is to numerically determine the optimal location of sensors for predicting the vibrational behavior of a wing. The methodology to achieve this goal will be to construct, using as starting point finite element simulations, a reduced-order model able to capture the essential vibrational characteristic of the wing.

2. Scope of the Project

1. Literature review
   - Elastodynamic Finite Element theory.
   - Model-order reduction (MOR)
     - Review of the different MOR methods.
     - General review on projection-based MOR.
   - Study the application of the MOR methods to aircraft structures.
   - Tetrahedral element.
   - Optimized cubature algorithms.

2. Study the geometry of a given isotropic wing configuration discretized using tetrahedral elements
   - Understand the joints among the different parts of the structure.
   - Understand the meshing.

3. Use an in-house finite element code (MATLAB) to obtain the different vibrational modes of the wing (vibrational behavior).
   - Develop a program to extract mass matrices and stiffness matrices at all Gauss points of the structure needed to obtain the natural vibrational modes of the wing.

4. Formulate the reduced-order model using modal analysis
   - Obtain the dominant vibrational modes of the wing.
   - Devise a strategy to treat boundary conditions.

5. Choose optimal location of integration points for internal forces using an “optimized cubature” algorithm. These locations can be regarded as the optimal positions of sensors for monitoring the structural behavior of the wing.

- Code existing optimization algorithms for addressing the issue of how to select a set of m points among the M Gauss points of the underlying mesh (M >> m).

6. Results validation

3. Requirements

- The code used for both the full-order numerical simulation and the model-order reduction will be developed using MATLAB.

- Projection-based model-order reduction method: the code must use as a Model-Order Reduction (MOR) method the “Single Value Decomposition (SVD)”.

3.1. Milestone specifications

- Obtain the main vibrational modes of the wing.
- Formulate the reduced-order model.
- Choose optimal location of integration points (sensor location).
- Validation.

4. Background

The structure of planes is tightly bonded to a set of tensional states that vary continuously depending on multiple input variables, most of them non-controllable by the pilot. These variations of loads and vibrations that the structure suffers from are especially noticeable in the wing, due to its characteristic shape and slenderness.

It is very useful to monitor all these different tensional states and vibrations to which the wing is submitted at all time during flight. Being aware it, allows to immediately determine whether the structure can be at any point on the verge to suffer any stress to which it has not been designed for and, consequently, perform the needed modifications in flight regime to avoid any type of material damage, which could lead to much bigger problems.

Due to the fact that it is not optimal to monitor the structure point by point, sensors are placed in characteristic points. From the information collected and by using post-processing algorithms, it is possible to obtain the tensional state and the vibration of the entire wing. The present project aims to study the optimal location of wing sensors using model-order reduction in a given wing geometry.

This technique is based on the finite element theory (FEM). The FEM was first created to solve structural problems in the aerospace industry and, due to its ease when it comes to programming and adaptability, it has evolved not only to other aerospace-study environments such as fluid dynamics or heat transfer, but to other disciplines as far from the engineering world as the film industry as well. (Kim and James 2011)

Even though nowadays computer technology is taking giant steps, the aerospace industry needs the obtained results to be very precise and trustworthy in order to improve designs. Acquiring these results requires using a highly-detailed discretization of the problem that leads to important calculating times.

In order to substantially decrease these calculating times compromising minimally the validity of the results, model-order reduction techniques come up (Lieu et al. 2006), for example the proper orthogonal decomposition (POD), or its discrete counterpart, the SVD that will be used during this project.

All these immediate computations regarding the state of the aircraft are becoming increasingly interesting in an industry where a lot of effort is being put into unmanned vehicles (UAV) and in the so-called "self-aware aerospace vehicles". These type of aircrafts can dynamically adapt the way they perform by gathering information about themselves and their surroundings and responding intelligently.

In (Allaire et al. 2014), the concept of an aircraft that can autonomously sense its structural state and dynamically re-plan its mission according to its current structural health is presented. This type of project, or other similar ones, use the advantages the Reduced Order Models offer to obtain accurate-enough results immediately.

In the present project, the Empirical Cubature Method (Hernández et al. 2016) is presented as a way of computing a Hyper-Reduced Order Model that could be perfectly used in the cutting-edge technology that are UAVs and self-aware aerospace vehicles. With this methodology, just by knowing the local properties of the structure at specifically chosen points, the overall structural behavior can be almost immediately approximated.

5. State of the art

Aerospace engineering is characterized for being a cutting-edge and innovative industry that always tries to be at the forefront of technology. The main companies spend a large part of their budget to research and develop new aerospace vehicles, equipment or processes to achieve optimal results and more relevant products.

The Incorporation of Finite Element studies was a breakthrough in the sector decades ago. Thanks to these studies, many of the configurations tested are discarded before having to build a prototype saving companies both time and money.

The need to obtain very reliable simulations and the complexity and nonlinearity of the equations that must be solved when designing a spacecraft caused these initial finite element models become obsolete due to the long calculation times.

Formerly, problems involving only one type of physical discipline were studied. That is, one could study the airflow and the forces that appear around a given geometry. Then use the results obtained in other studies (ran apart), where these forces previously calculated were taken as input parameters, and the behavior of the structure could be studied.

Nowadays, it is becoming increasingly used the model called "Multiphysics", in which in the same finite-element study, different physical disciplines such as aerodynamics and structural aspects are involved. This way one can better understand how the geometry interacts with the flow and get better results that will build better aeronautical vehicles. However, such multiphysics processes require large computational power. For this reason, different model-order reduction techniques joined the industry to mitigate these computational loads.

Since then, the various ROM have been used in multiple projects and aeronautical studies. From modeling of a complete F-16 fighter configuration, in order to assess its potential for the solution of realistic aeroelastic problems (Lieu et al. 2006), to more recent items like Numerical Simulation and Reduced-Order Aerodynamic Modeling of a Lambda Wing Configuration (Ghoreyshi et al. 2016).

In addition, the results obtained by these ROMs are accepted by the industry as accurate (Lieu et al. 2006): *"it was recently shown that ROMs constructed by a variety of methods, including the popular proper orthogonal decomposition (POD) method, can produce numerical results that compare well with those generated by full-order nonlinear models."*

This project wants to go one step further and uses the methodology presented in (Hernández et al. 2016) to create a hyper-reduced model able to obtain the vibration modes without committing any error in the approximation. In addition, the low number of integration points needed in the hyper-reduced model helps obtaining the results almost immediately.

6. Problem approach

6.1. Introduction to dynamic modelling of structures

Structural dynamics is an engineering branch that allows the study of the behavior of structures subject to any type of dynamic excitement, either continuous or transient (Arcos 2015).

Except for the case of collisions, the dynamic forces are usually inferior than the static stresses. In the aeronautical field, the most common dynamic excitations that can affect the aircrafts are:

- Aerodynamic excitation, studied using dynamic aeroelasticity.
- Structural excitation. Coming mainly from the aircraft's engines.

The deformations generated by these dynamic excitations can usually be considered within the small deformation theory. This means that the systems analyzed can be considered as lineal.

Structural dynamics is a science and engineering discipline that was first initiated in 1877 with the publication of the book *The Theory of Sound* by Lord Rayleigh. Since its creation, structural dynamics has studied how to foresee the dynamic behavior from structures such as aircrafts, vehicles, machinery, buildings… always with the objective of controlling the possible negative outcomes that high levels of vibration could generate: structural collapse, fatigue, system instabilities and efficiency loss among others.

In order to predict this dynamic behavior previously introduced, structural dynamics has developed two big modelling methodologies:

- **Numerical methodology:** used when the study is needed on a non-existent structure, real prototype or in-scale prototype.

- **Experimental methodology:** used when the study is needed on an existent structure, real prototype or in-scale prototype. This one also includes the numerical methodology in the process.

In this project, the numerical methodology will be. The finite element method (FEM) is going to be used. The FEM formulation for classical linear elastodynamics will be explained in the next section.

6.2. Finite element method formulation

It will be assumed that the reader has a basic understanding of the Finite Element Theory formulation for linear elastostatic problems, since the formulation for the linear elastodynamic problem will be considered as an extension of the elastostatic one. The formulation is explained following the discussion in (Hughes 1987) and the class notes from professor Joaquín Hernández (Hernández 2015).

6.2.1. Preliminaries

In the elastodynamic formulation, accelerations, inertial forces and damping among other parameters have to be considered. The modifications with respect to the linear elastostatic formulation are the following:

1) When formulating the **Cauchy stress tensor** σ_{ij} $(i,j = 1, \dots n_{sd})$ at a given time, a dependency with the time derivative of the strain tensor ε_{ij} must be added.

$$\boldsymbol{\sigma}(t) = \boldsymbol{C}\boldsymbol{\varepsilon}(t) + \boldsymbol{D}\dot{\boldsymbol{\varepsilon}}(t) \quad (1)$$

Where:

- $\boldsymbol{C}$ is the tensor of elastic coefficients.
- $\boldsymbol{D}$ is the tensor of viscoelasticity coefficients. It is typically assumed that $\boldsymbol{D} = \beta\boldsymbol{C}$. This means that the viscoelastic coefficients are

proportional to the elasticity coefficients. The **damping coefficient** β is usually taken uniform over the body (the same for all finite elements).

Compared to the elastostatic problem, it can be seen that a term that is not proportional to the deformation per se is added. $\dot{\boldsymbol{\varepsilon}}(t) = \frac{d\boldsymbol{\varepsilon}}{dt}$ depends on the speed of application. If the forces are applied very slowly, the strain speed tends to zero and the elastostatic Cauchy stress tensor is obtained.

2) Regarding the **body forces** per unit of volume $\boldsymbol{f_i}$, new terms such as an **inertia term** (proportional to acceleration) and a **damping term** (proportional to velocity) are added.

$$\boldsymbol{f_i} \rightarrow \boldsymbol{f_i} - \rho\ddot{\boldsymbol{u}}_{\boldsymbol{i}} - \overline{\mu}\dot{\boldsymbol{u}}_{\boldsymbol{i}} \qquad (2)$$

Where:

- $-\rho\ddot{\boldsymbol{u}}_{\boldsymbol{i}}$ corresponds to the inertial forces. ρ is the density of the unit of volume and $\ddot{\boldsymbol{u}}_{\boldsymbol{i}} = \frac{\partial^2 \boldsymbol{u}_i}{\partial t^2}$ is the acceleration of deformation.
- $-\overline{\mu}\dot{\boldsymbol{u}}_{\boldsymbol{i}}$ corresponds to the damping forces. $\overline{\mu}$ is the damping parameter. It is usually defined as $\overline{\mu} = \overline{\alpha}\rho$, where $\overline{\alpha}$ is another damping coefficient such as β before, also normally considered constant. $\dot{\boldsymbol{u}}_{\boldsymbol{i}} = \frac{\partial u_i}{\partial t}$ is the velocity of deformation.

Then again, if the external forces to the structure are applied very slowly, $\dot{\boldsymbol{u}}_{\boldsymbol{i}} \rightarrow 0$ and $\ddot{\boldsymbol{u}}_{\boldsymbol{i}} \rightarrow 0$. Then the elastostatic body-force expression is obtained.

These are the modifications with respect to linear elastostatics that have to be considered when formulating the elastodynamic FE problem.

6.2.2. Boundary conditions

It is crucial to correctly determine the boundary conditions. To do so, it will be assumed that the boundary Γ can be decomposed into two different boundaries.

$$\Gamma = \Gamma_u^i \cup \Gamma_\sigma^i \tag{3}$$

Where

$$\Gamma_u^i \cap \Gamma_\sigma^i = \emptyset \tag{4}$$

The index i goes from 1 to the number of spatial dimensions n_{sd}. In a 3D case, as the one in this project, $n_{sd} = 3$.

Another consideration concerning the boundary is that this decomposition previously made does not change over time. This means that all the nodes that were initially in one of the two boundaries will remain in that boundary during all of the study.

This boundary decomposition will be used to select the nodes in which the different boundary conditions of the problem are placed. The nodes with prescribed displacement (Dirichlet boundary conditions) will be the ones in Γ_u^i, while tractions are prescribed on boundaries Γ_σ^i (Neumann boundary conditions). The set of restricted degrees of freedom (global degrees of freedom along which displacement is known) will be denoted as the set $\boldsymbol{r}$, while the set of unconstrained degrees of freedom (global degrees of freedom along which the displacement is unknown) will be denoted as $\boldsymbol{l}$.

Note that even though these boundaries do not change over time, both the value of the displacements on the restricted nodes and the value of the tractions on the Neumann boundaries may. This means that the boundary conditions (displacements or tensions) at all time steps and at all nodes must be provided in order to define the problem.

To complete the description of the problem, the initial conditions must be given. Unlike in elastostatic problems, in elastodynamics it is necessary to determine the initial conditions for both the displacement $u_{\mathrm{i}}(\boldsymbol{x},0)$ and velocities $\dot{u}_{\mathrm{i}}(\boldsymbol{x},0)$.

$$u_{\mathrm{i}}(\boldsymbol{x},0) = u_i^0(\boldsymbol{x}) \tag{5}$$

$$\dot{u}_{\mathrm{i}}(\boldsymbol{x},0) = \dot{u}_i^0(\boldsymbol{x}) \tag{6}$$

6.2.3. Finite element formulations (global point of view)

The formulation of the set of ordinary differential equations to be reduced is presented below. Of course, it is the standard finite element, semi-discrete motion equation for elastodynamic problems in its Lagrangian form:

$$\boldsymbol{M_{ll}\ddot{d}_l + D_{ll}\dot{d}_l + K_{ll}d_l = F_l} - (\boldsymbol{M_{lr}\ddot{\overline{u}} + D_{lr}\dot{\overline{u}} + K_{lr}\overline{u}}) \tag{7}$$

$$\boldsymbol{d_l}(0) = \boldsymbol{d_l^0} \tag{8}$$

$$\dot{\boldsymbol{d}}_{\boldsymbol{l}}(0) = \dot{\boldsymbol{d}}_{\boldsymbol{l}}^{\boldsymbol{0}} \tag{9}$$

For the sake of notational simplicity, the notation is redefined leaving the previously explained boundary notation aside. The super index h is added to denote that the vectors and matrices belong to the full order model (FE analysis). When formulating the reduced order model, this super index will disappear.

$$\boldsymbol{d_l} \to \boldsymbol{d}^h \qquad \boldsymbol{M_{ll}} \to \boldsymbol{M}^h \qquad \boldsymbol{D_{ll}} \to \boldsymbol{D}^h \qquad \boldsymbol{K_{ll}} \to \boldsymbol{K}^h$$

$$\boldsymbol{F_l} - \left(\boldsymbol{M_{lr}\ddot{\overline{u}} + D_{lr}\dot{\overline{u}} + K_{lr}\overline{u}}\right) \to \boldsymbol{F}_{ext}^h \qquad \boldsymbol{d_l^0} \to \boldsymbol{d}^{0^h} \qquad \dot{\boldsymbol{d}}_{\boldsymbol{l}}^{\boldsymbol{0}} \to \dot{\boldsymbol{d}}^{0^h}$$

Then, Equation (7) can be rewritten as:

$$\boldsymbol{M}^h\ddot{\boldsymbol{d}}^h + \boldsymbol{D}^h\dot{\boldsymbol{d}}^h + \boldsymbol{K}^h\boldsymbol{d}^h = \boldsymbol{F}_{ext}^h \tag{10}$$

Here, $\boldsymbol{d}^h \in \mathbb{R}^N$ (N = number of FE nodes) denotes the vector of unknown nodal displacements. The superposed dots in $\dot{\boldsymbol{d}}^h$ and $\ddot{\boldsymbol{d}}^h$ indicate material time derivative, i.e. unknown nodal velocity $\dot{\boldsymbol{d}}^h = \frac{\partial \boldsymbol{d}^h}{\partial t}$ and unknown nodal acceleration $\ddot{\boldsymbol{d}}^h = \frac{\partial^2 \boldsymbol{d}^h}{\partial t^2}$. $\boldsymbol{M}^h \in \mathbb{R}^{NxN}$, $\boldsymbol{D}^h \in \mathbb{R}^{NxN}$ and $\boldsymbol{K}^h \in \mathbb{R}^{NxN}$ denote the mass, damping and stiffness matrices respectively. Finally, $\boldsymbol{F}_{ext}^h$ represents the vector of nodal external forces.

Notice that the vector of nodal internal forces $\boldsymbol{F}^h$ can be calculated as

$$\boldsymbol{F}^h = \boldsymbol{D}^h \dot{\boldsymbol{d}}^h + \boldsymbol{K}^h \boldsymbol{d}^h \tag{11}$$

6.2.3.1. Modal decomposition analysis: undamped free vibration problem

In *Section 6.2.3*, the finite element formulation for the linear elastodynamic problem has been presented. However, to accomplish this project's objective, only the normal modes of the structure need to be obtained.

A normal mode of an oscillating system is a pattern of motion in which all parts of the system move sinusoidally with the same frequency and with a fixed phase relation. The free motion described by the normal modes takes place at fixed frequencies. These fixed frequencies of the normal modes of a system are known as its natural frequencies. A physical object, such as a building, bridge or molecule, has a set of normal modes and their natural frequencies that depend on its structure, materials and boundary conditions.

A mode of vibration is characterized by a modal frequency and a mode shape (Arcos 2015). In order to calculate these modal frequencies and mode shapes, the undamped free vibration problem must be solved ($\boldsymbol{D}^h = \boldsymbol{0}, \boldsymbol{F}^h = \boldsymbol{0}$). This means that Equation (10) is reduced to:

$$\boldsymbol{M}^h \ddot{\boldsymbol{d}}^h + \boldsymbol{K}^h \boldsymbol{d}^h = \boldsymbol{0} \tag{12}$$

Given the initial conditions $\boldsymbol{d}(0) = \boldsymbol{d^0}$ and $\dot{\boldsymbol{d}}(0) = \dot{\boldsymbol{d}}^{\boldsymbol{0}}$, $\boldsymbol{d}$ at all time steps and elements must be calculated. Equation (12) can be rewritten in the frequency domain to ease its resolution.

$$(-\omega^2\, \boldsymbol{M}^h + \boldsymbol{K}^h)\boldsymbol{\Phi} = \boldsymbol{0} \tag{13}$$

Where $\boldsymbol{\Phi}$ is the vibrational displacement vector for each mode and it is defined as

$$\boldsymbol{\Phi} = \{\boldsymbol{\Phi_1}\ \boldsymbol{\Phi_2}\ \dots\ \boldsymbol{\Phi_N}\}^{\mathrm{T}} \tag{14}$$

The initial conditions also need to be converted to the frequency domain as $q_i^0 = \boldsymbol{\Phi_i^T d^0}$ and $\dot{q_i^0} = \boldsymbol{\Phi_i^T \dot{d}^0}$

The non-trivial solution of Equation (13) is determined by the set of P values λ, known as eigenvalues, that fulfill the following expression:

$$\det(-\lambda \boldsymbol{M}^h + \boldsymbol{K}^h) = \boldsymbol{0} \tag{15}$$

Where $\lambda = \omega^2$. By substituting any of these eigenvalues $\lambda_i\ i = (1, 2, \dots, P)$ to Equation (13), the expression is written as:

$$(-\lambda_i \boldsymbol{M}^h + \boldsymbol{K}^h)\boldsymbol{\Phi}_{\mathrm{i}} = \boldsymbol{0} \tag{16}$$

Now $\boldsymbol{\Phi}_{\mathrm{i}}$ is the eigenvector associated to the eigenvalue λ_i and, consequently, to the natural frequency ω_i. This natural frequency along with the eigenvector $\boldsymbol{\Phi}_{\mathrm{i}}$ define the normal mode i. The free movement of the system under study will be a superposition of all these P normal modes, each one of them generating a movement inside the system (depending on its eigenvector), and vibrating at its corresponding associated natural frequency. The solution of the problem can be written as:

$$\boldsymbol{d} = \sum_{i=1}^{\boldsymbol{P}} \boldsymbol{\Phi}_i \left(q_i^0 \cos \omega_i t + \frac{\dot{q_i^0}}{\omega_\mathrm{i}} \sin \omega_i t \right) \tag{17}$$

$\boldsymbol{\Phi}_i$ are assumed to be scaled so that $\boldsymbol{\Phi}_i^T \boldsymbol{M}^h \boldsymbol{\Phi}_i = 1$.

6.2.4. Element point of view

As it can be seen in Equation (12), the full order mass and stiffness matrices need to be computed in order to solve the problem. In this section these two matrices are assembled.

The procedure will follow the physical definition of the Finite Element method. The basic concept in the physical interpretation is the breakdown of a complex mechanical system into simpler, disjoint components called finite elements, or simply elements.

The mechanical response of an element is characterized in terms of a finite number of degrees of freedom. These degrees of freedom are represented as the values of the unknown functions at a set of node points, in the case of this project, displacements.

The response of the original system is considered to be approximated by that of the discrete model constructed by connecting or assembling the collection of all elements.

6.2.4.1. *Assembly of the global stiffness matrix*

Following the physical definition of the FE method, the global stiffness matrix is calculated as the assembly of the contribution of each elemental stiffness matrix.

$$\boldsymbol{K}^h = \bigwedge_{e=1}^{n_{el}} \boldsymbol{K}^e = \sum_{e=1}^{n_{el}} \boldsymbol{L}^{e^T} \boldsymbol{K}^e \boldsymbol{L}^e \tag{18}$$

Where n_{el} is the number of elements, $\boldsymbol{K}^e$ denotes each elemental stiffness matrix and $\boldsymbol{L}^e$ is the Boolean matrix of each element.

The element stiffness matrix $\boldsymbol{K}^e$ can be calculated by means of Equation (19)

$$\boldsymbol{K}^e = \int_{\Omega^e} \boldsymbol{B}^{e^T} \boldsymbol{C} \boldsymbol{B}^e d\Omega^e \tag{19}$$

Here, $\boldsymbol{B}^e$ is the symmetric gradient of shape functions (depends on the type of element) and $\boldsymbol{C}$ is the elasticity matrix. This last one, for isotropic materials and in 3D, reads as follows.

$$C = \begin{bmatrix} \lambda+2\mu & \lambda & \lambda & 0 & 0 & 0 \\ \lambda & \lambda+2\mu & \lambda & 0 & 0 & 0 \\ \lambda & \lambda & \lambda+2\mu & 0 & 0 & 0 \\ 0 & 0 & 0 & \mu & 0 & 0 \\ 0 & 0 & 0 & 0 & \mu & 0 \\ 0 & 0 & 0 & 0 & 0 & \mu \end{bmatrix} \tag{20}$$

Where λ and μ stand for the Lame parameters, which are functions of the Young's modulus (E) and the Poisson's coefficient (ν) of the material.

$$\lambda = \frac{\nu E}{(1+\nu)(1-2\nu)}; \qquad \mu = \frac{E}{2(1+\nu)} \tag{21}$$

The integral in Equation (19) is calculated in the full order analysis via Gauss quadrature.

$$\boldsymbol{K}^e = \int_{\Omega^e} \boldsymbol{B}^{eT} \boldsymbol{C} \boldsymbol{B}^e d\Omega^e = \sum_{g=1}^{M} \omega_g J^e \boldsymbol{B}^{eT}(\boldsymbol{x}_g) \boldsymbol{C}(\boldsymbol{x}_g) \boldsymbol{B}^e(\boldsymbol{x}_g) \quad (22)$$

$\boldsymbol{x}_g \in \Omega$ denotes the position of the g-th integration point, ω_g the corresponding weights and J^e the Jacobian of the finite element containing the integration point.

6.2.4.2. Assembly of the global mass matrix

The mass matrix is assembled the same way as the stiffness matrix, only that the elemental Mass matrix is defined differently. First, the global mass matrix can be calculated as the assembly of the contribution of each elemental mass matrix.

$$\boldsymbol{M}^h = \bigwedge_{e=1}^{n_{el}} \boldsymbol{M}^e = \sum_{e=1}^{n_{el}} \boldsymbol{L}^{eT} \boldsymbol{M}^e \boldsymbol{L}^e \quad (23)$$

Now, the elemental mass matrix $\boldsymbol{M}^e$ is calculated as follows:

$$\boldsymbol{M}^e = \int_{\Omega^e} \rho \boldsymbol{N}^{eT} \boldsymbol{N}^e d\Omega^e \quad (24)$$

Where ρ is the density of each element and $\boldsymbol{N}^e$ is the matrix of shape functions (depends on the type of element).

Again, the integral in Equation (24) is calculated via Gauss quadrature

$$\boldsymbol{M}^e = \int_{\Omega^e} \rho \boldsymbol{N}^{eT} \boldsymbol{N}^e d\Omega^e = \sum_{g=1}^{M} \omega_g J^e \rho \boldsymbol{N}^{eT}(\boldsymbol{x}_g) \boldsymbol{N}^e(\boldsymbol{x}_g) \quad (25)$$

6.3. Model-order reduction methods (MOR)

Model-order reduction methods are techniques designed to reduce the computational complexity of dynamical systems described by a set of ordinary or differential algebraic equations, i.e. to come up with a simpler model from a more complex one without compromising the accuracy of the results obtained. The simpler model is referred to as the "Reduced-order model (ROM)", while the more complex model from which the ROM originates is the "full-order model". In the case of this project, the full-order model is a Finite Element (FE) model.

The necessity to formulate this reduced-order models arises from the fact that nowadays, even though the capabilities from computers are evolving exponentially, the discretization in space and time of the finite element models leads to a high-dimensional system very costly to solve timewise speaking. The goal of model order reduction is to find a low-dimensional but accurate approximation of the large-scale dynamic system. This way one can drastically reduce time required to calculate the model maintaining the validity of the results.

One of the model order reduction techniques that is most commonly used in structural analysis and the one that this project will use is the Proper Orthogonal Decomposition (POD) or its discrete counterpart the Single Value Decomposition (SVD).

6.3.1. Review and formulation of the POD and SVD

The Proper Orthogonal Decomposition (POD) can be classified inside the projection-based reduced-order models. This method has been used to produce a reduced-order model in different fields such as low-dimensional descriptions of turbulent fluid flows, damage detection or structural vibrations to name a few. Apart from scientific or engineering purposes, it has also been extensively used in signal analysis, data compression or image processing (Chatterjee 2000).

The POD is often used to extract basis functions or mode shapes that can approximate a function over some domain of interest. Suppose we want to approximate a function $z(x,t)$ as a finite sum of variables:

$$z(x,t) \approx \sum_{k=1}^{M} a_k(t)\phi_k(x) \tag{26}$$

This approximation is not unique and could be done using an infinite number of different functions. For every $\phi_k(x)$ there could be an $a_k(t)$ able to correctly approximate the function.

In the POD, the functions $\phi_k(x)$ are chosen to be orthogonal basis functions, that is

$$\int_{\boldsymbol{X}} \phi_{k_1}(x)\phi_{k_2}(x)\mathrm{dx} = \begin{cases} 1 \; if \; k_1 = k_2 \\ 0 \; otherwise \end{cases}$$

Then,

$$a_k(t) = \int_{\boldsymbol{X}} z(x,t)\phi_k(x)dx \tag{27}$$

It can be seen that the determination of $a_k(t)$ depends only on $\phi_k(x)$. The criteria to determine the sequence of orthonormal functions $\phi_k(x)$ is such that the first M of these functions give the best M-term approximation of the initial function of $z(x,t)$.

Once the $\phi_k(x)$ and $a_k(t)$ functions are determined this way, the expression in Equation (26) is called the POD of $z(x,t)$.

For the finite-dimensional case, i.e. cases in which the value of the function willing to be approximated is only known at discrete points in the domain (Finite Element problems) the Proper Orthogonal Decomposition is computed as the Single Value Decomposition.

Imagine the different values of $z(x,t)$ arranged in a $N\ x\ m$ matrix $\boldsymbol{A}$ such that the element A_{ij} corresponds to the value $z(x_i, t_j)$. The Single Value Decomposition of the matrix $\boldsymbol{A}$ consists in approximating A as a multiplication of three matrices $\boldsymbol{U}, \boldsymbol{\Sigma}$ and $\boldsymbol{V}$.

$$\boldsymbol{A} = \boldsymbol{U}\boldsymbol{\Sigma}\boldsymbol{V}^{\boldsymbol{T}} \tag{28}$$

Where $\boldsymbol{U}$ and $\boldsymbol{V}$ are NxN and $m\ x\ m$ orthogonal matrices respectively, the superscript T indicates matrix transpose, and $\boldsymbol{\Sigma}$ is an $N\ x\ m$ diagonal matrix. The elements from the diagonal consist of $r = \min(N, m)$ nonnegative numbers σ_j arranged in decreasing order. These values from the diagonal are called the Singular Values of $\boldsymbol{A}$.

This SVD technique will be later on used in the project for determining the orthogonal basis matrix $\boldsymbol{\Lambda}$ from the matrix of zero-integral snapshots $\widehat{\boldsymbol{X}}_{\boldsymbol{\mathcal{F}}}$, obtained from the reduced internal forces at all integration points and training configurations $\boldsymbol{X}_{\boldsymbol{\mathcal{F}}}$.

6.4. Optimized cubature algorithms

The finite element formulation in *Section 6.2.3* lead us to the Equation (11) where $\boldsymbol{F}^h \in \mathbb{R}^N$ denoted the vector of FE nodal internal forces. The FE integration rule employed to evaluate this vector is the Gauss quadrature, characterized by the gauss integration points and weights.

$$\boldsymbol{F}^h = \int_\Omega \boldsymbol{f}^h \, d\Omega \approx \sum_{g=1}^{M} \omega_g J^e \boldsymbol{f}^h(\boldsymbol{x}_g) = \sum_{g=1}^{M} W_g \boldsymbol{f}^h(\boldsymbol{x}_g) \tag{29}$$

Again, $\boldsymbol{x}_g \in \Omega$ denotes the position of the g-th integration point, ω_g the corresponding weights and J^e the Jacobian of the finite element containing the integration point. $W_g = \omega_g J^e$.

Now, let $\boldsymbol{F} \in \mathbb{R}^n$ represent the projection onto the reduced order space of $\boldsymbol{F}^h$ ($n \ll N$). These two vectors can be related using the matrix of basis vectors $\boldsymbol{\Phi} \in \mathbb{R}^{Nxn}$ ($\boldsymbol{F} = \boldsymbol{\Phi}^T \boldsymbol{F}^h$). This basis vectors $\boldsymbol{\Phi}$ will be computed as the vibrational modes matrices in the sensor location problem.

In order to approximate $\boldsymbol{F}$, an integral approach approximation is going to be followed. More specifically, a cubature method (An et al. 2008).

In a finite element context, $\boldsymbol{F}$ can be obtained not only by projecting the FE nodal internal forces into a reduced-order space ($\boldsymbol{F} = \boldsymbol{\Phi}^T \boldsymbol{F}^h$), but also by integrating over the domain the corresponding reduced-order variable $\boldsymbol{f} = \boldsymbol{\Phi}^T \boldsymbol{f}^h$.

$$\boldsymbol{F} = \boldsymbol{\Phi}^T \boldsymbol{F}^h = \boldsymbol{\Phi}^T \int_\Omega \boldsymbol{f}^h d\Omega = \int_\Omega \boldsymbol{f} \, d\Omega \tag{30}$$

This means that the reduction problem can be regarded as the approximation of an integral instead of the approximation of a vector. To approximate the integral, a similar

method as the one used to compute the FE nodal internal forces itself will be followed. The integral is going to be approximated as a weighted sum of the integrand evaluated at optimal sampling points.

$$\boldsymbol{F} \approx \sum_{g=1}^{m} \omega_g \, \boldsymbol{f}(\bar{\boldsymbol{x}}_g) \tag{31}$$

This strategy consists in determining, among the integration points of the FE mesh, a reduced set of m points and associated positive weights ω so that the integration error is minimized. The reason why the weights have to be positive is that, in a structural problem as the one in this project, if the FE stiffness matrix is symmetric and positive, so will be its reduced-order counterpart.

6.5. Sensor location

Via the m integration points and their associated weights it will be possible to build a reduced-order model capable of computing accurately and almost immediately the vibrational modes and frequencies of the geometry under study.

The main objective of the present study is to determine the optimal location of wing sensors using model-order reduction. The location of these wing sensors is going to be considered as the location in the geometry of the optimal integration points, due to their property of correctly reconstructing the vibrational state of the structure even though the information is only available at certain points (just as physical sensors do).

7. Geometry description

7.1. Geometry presentation

The geometry that will be studied in this project can be seen in Figure 1. It is a simplified version of a typical rectangular wing, where all the structural elements such as spars and stingers have been represented as a pair of long beams crossing all foils. This wing is 3 meters long and the airfoils have a chord of 150 cm. The airfoil used is NACA 4415. This geometry has been designed using the commercial software SolidWorks.

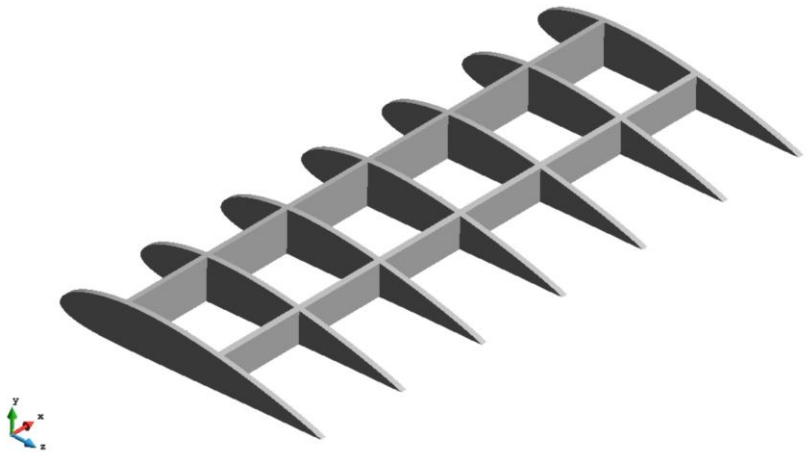

Figure 1 Geometry under study

7.2. Meshing

In order to perform a Finite Element analysis on this structure, the geometry needs to be meshed, i.e. discretized in a large number of small elements. By doing so, the final solution can be regarded as the assembly of each elemental contribution.

The wing will hold two different meshes: the mesh related to all the elements that are in the interior of the wing's geometry and the boundary mesh (mesh containing all the elements that are in the surface).

The geometry can be meshed using different types of element (tetrahedral element, hexahedral element, shell element…). Since the geometry under study is mainly formed by an assembly of thin plates, the ideal finite element to make the mesh with is the shell element.

However, the development of a finite element code capable of computing stresses and strains, as well as vibrational modes using the shell element can be regarded as a complete project itself.

Instead, an academic finite element code will be used as starting point for the project. The downside of using this finite element code is that the geometry cannot be meshed with the shell element. In its place, elements with only three degrees of freedom can be used. This means that each element holds less unknowns (each degree of freedom is a potential unknown) but, since these type of elements are not able to rotate, to correctly determine the movement of the plates, a minimum of three elements have to be placed along its thickness. In summary, the computational power required to solve the same problem increases. This is the reason why the covering of the wing is not being considered, but just the interior structure instead. Bearing in mind the covering would increase by a lot the number of elements needed. Furthermore, the computational effort and solving time would be too high. However, it is important to emphasize that

the methodology followed during this project is applicable to any geometry and the resolution time will only depend on the number of elements in the mesh.

Finally, the geometry is meshed using the tetrahedral element for the interior mesh and triangles for the boundary mesh, Figure 2 and Figure 3.

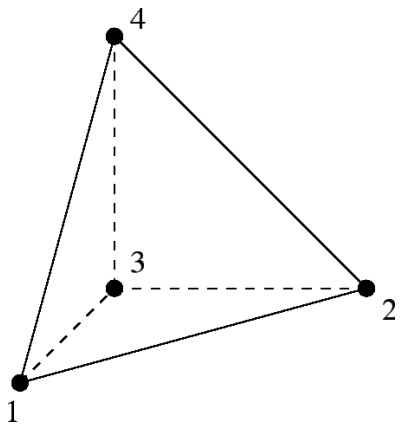

Figure 2 Tetrahedral element. Source: http://bit.ly/1UDVIHs

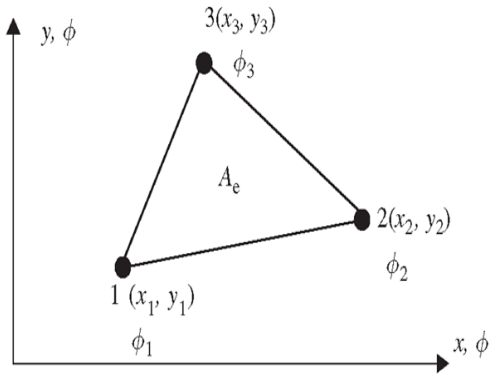

Figure 3 Triangular Element. Source: http://bit.ly/1YglyHp

To make sure that a minimum of three elements are placed along the thickness of each plate, the geometry is imported to GiD and a mesh of almost 550.000 elements is generated using GiD's meshing engine. Figure 4 to Figure 6 show the contour mesh for the geometry discretized using 200.000, 550.000 and 900.000 elements respectively. It is important to emphasize that with 200.000 elements there are areas where there are less than three elements along the thickness. This problem is solved in both of the other meshes.

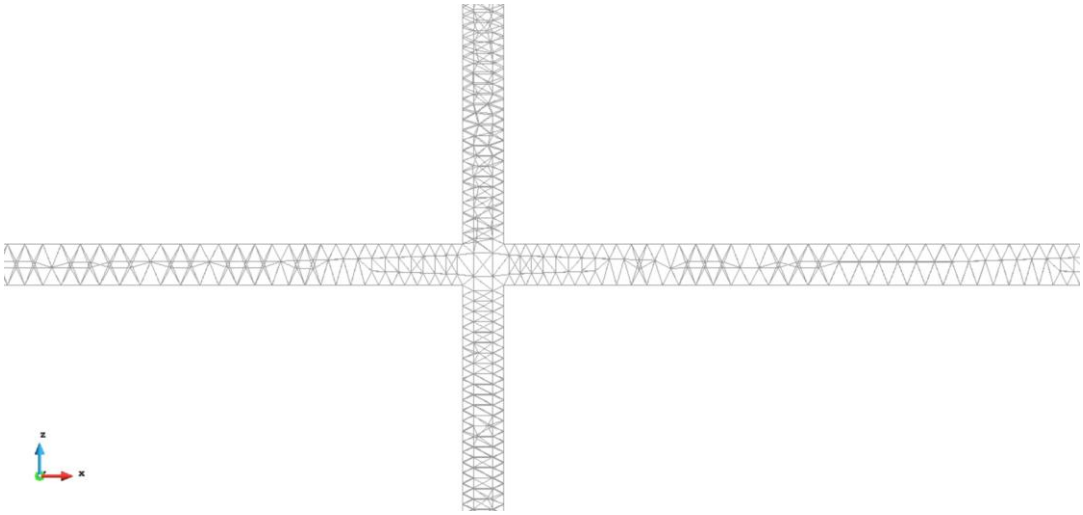

Figure 4 200.000-element mesh

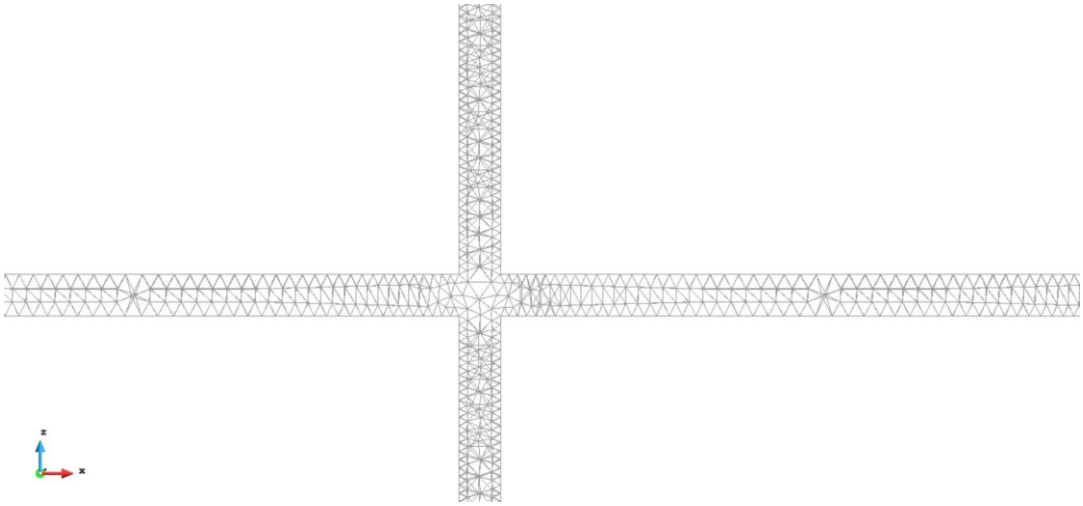

Figure 5 550.000-element mesh

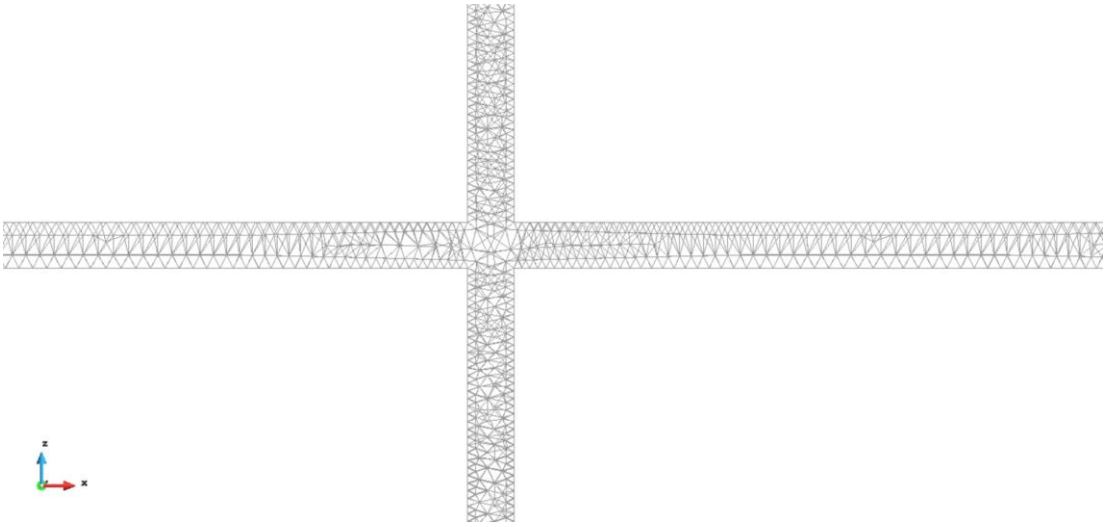

Figure 6 900.000-element mesh

The final decision of how many elements are used in the mesh relies on the difference of natural frequencies obtained in the modal study. In Table 1 the different natural frequencies for the different modes using different numbers of elements in each discretization is shown. What is more, under each column appears the approximated computing time for each mesh. All the calculations were performed in a laptop running at 3.5 GHz with 16 GB of RAM and 4 *Intel Core-i7* processors, in OS X.

	Natural frequencies (rad/s)				
Elements	70.000	100.000	200.000	550.000	900.000
Mode 1	74,52	73,87	73,48	73,01	72,64
Mode 2	94,88	87,18	84,36	77,85	73,75
Mode 3	153,69	141,30	136,76	127,56	121,41
Mode 4	298,81	273,70	265,13	243,89	230,96
Mode 5	437,11	425,61	420,39	409,90	402,16
Mode 6	540,25	493,33	476,72	437,23	413,38
Computing time	24"	44"	1' 17"	3' 32"	7' 50"

Table 1. Natural frequencies for each mode obtained using an increasing number of elements per mesh

If the reference is set in the results obtained with the mesh that uses 900.000 elements (because the more elements, the more precise the results are), the relative difference in each natural frequency is shown in Table 2.

Relative difference (%)				
Elements	70.000	100.000	200.000	550.000
Mode 1	2,6%	1,7%	1,2%	0,5%
Mode 2	28,7%	18,2%	14,4%	5,6%
Mode 3	26,6%	16,4%	12,6%	5,1%
Mode 4	29,4%	18,5%	14,8%	5,6%
Mode 5	8,7%	5,8%	4,5%	1,9%
Mode 6	30,7%	19,3%	15,3%	5,8%

Table 2 Relative difference in each natural frequency with respect to the values obtained with the 900.000-element mesh

It can be seen how the results obtained with the mesh of 550.000 elements vary a maximum of less than a 6% with respect to the reference mesh. Additionally, the computing time of the FE problem is halved.

What is more, in later stages of the project it was seen how an average computer would struggle dealing with the huge matrices that arose during all the calculations of the full-order model and ROM using the 550.000-element mesh. Hence, finer discretizations could not have been computed.

For these reasons, the mesh with 550.000 elements is used for the project. Even though more accurate results would be obtained with the 900.000 element mesh, the results with the selected mesh are good enough for the depth of this project. Figure 7 shows a close up of the selected mesh.

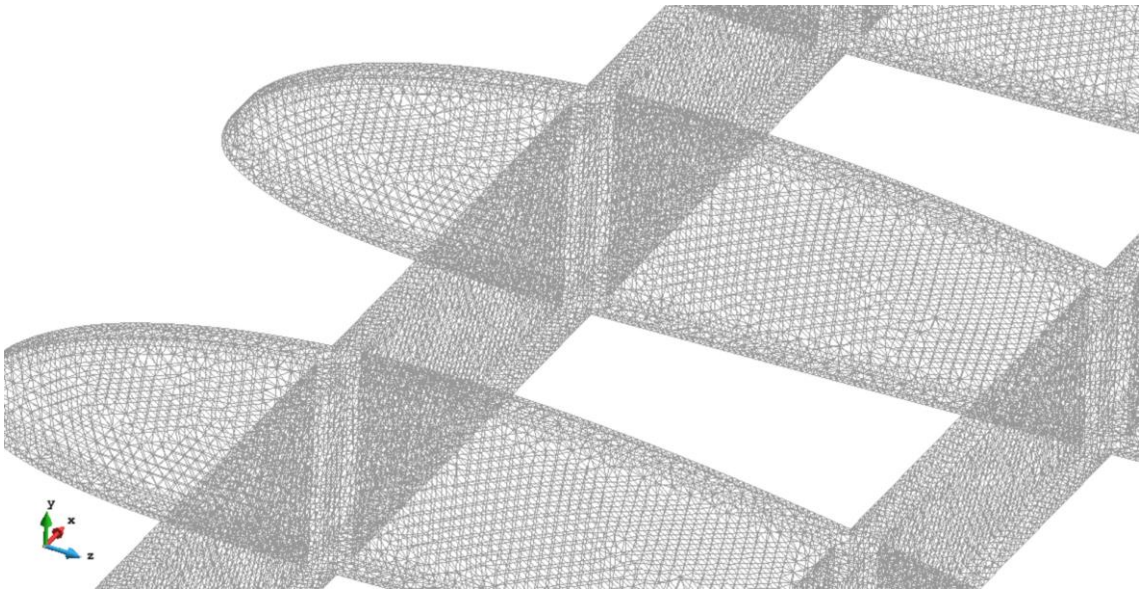

Figure 7 Close up of the 550.000-element mesh

As said before, the element used to discretize the geometry is the tetrahedral element. This means that the boundary mesh is made of triangular elements.

8. Vibrational modes

The first step towards the determination of the optimal integration points (that will be considered as the optimal sensor location for the wing) is obtaining the first P vibrational modes. In the case of this project, the first $P = 6$ vibrational modes will be calculated.

To perform the analysis, it will be assumed that the wing can't move from its leftmost end. Computationally it is as saying that the nodes located at the minimal "x" position have its movement in the three directions in space restricted and equal to zero. Moreover, to determine the natural frequencies the undamped free vibration problem has to be solved. This means that there are no external forces applied in the structure.

In a first approach, the interior structure of the wing is set to be isotropic made of aluminum. Since the problem is considered elastic, the behavior of the materials under stress can be modeled by its Young's modulus and Poisson's ratio, both set to be $E = 70\ MPa\ and\ \nu = 0.3$ respectively. The density of the material is set to be $\rho = 2.700\ kg/m^3$.

The exact number of elements in the mesh is $N_{elem} = 545.290$, and the number of nodes is $N_{node} = 120.281$. To calculate the stiffness matrix and the internal forces vector, a 2x2 Gauss integration rule will be used giving a total number of Gauss points of $M = 4N_{elem} = 2.181.160$.

As it has been explained in *Section 6.2.3.1 Modal decomposition analysis: undamped free vibration problem*, in order to obtain each of the six modes of vibration and its natural frequencies, the Equation (12) has to be solved. Then, using GID[1]'s

[1] GiD is a pre and post processor for numerical simulations in science and engineering developed by the International Center for Numerical Methods in Engineering (CIMNE), linked to the Technical University of Catalonia (BarcelonaTech).

postprocessor, these natural modes can be plotted. Figure 8 to Figure 13 show these natural vibrational modes and its corresponding natural frequencies.

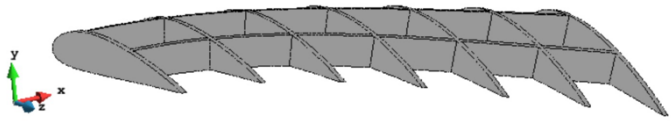

Figure 8 Mode 1: 73,01 rad/s

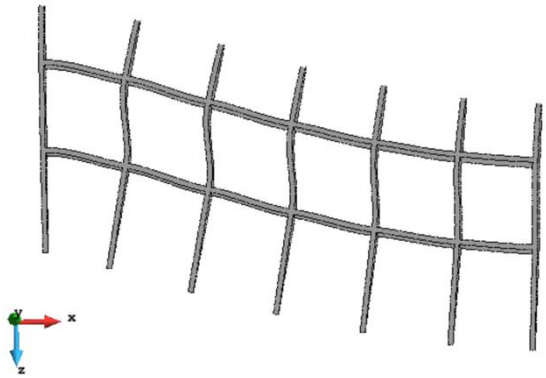

Figure 9 Mode 2: 77,85 rad/s

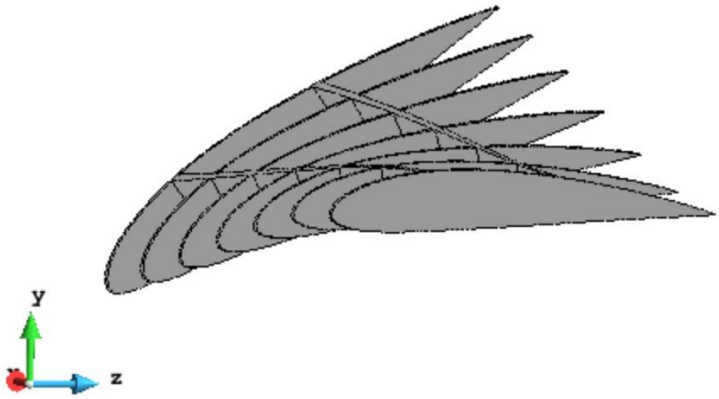

Figure 10 Mode 3: 127,56 rad/s

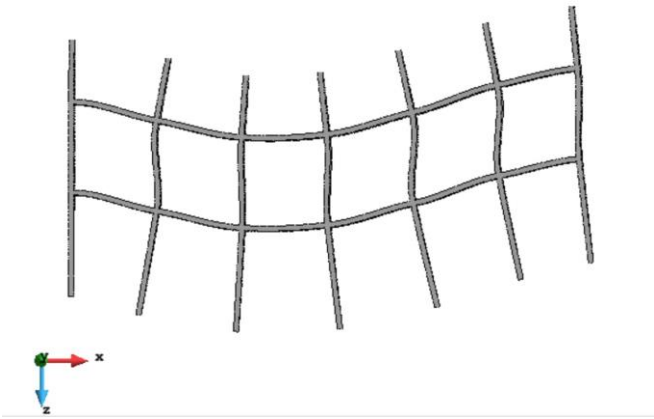

Figure 11 Mode 4: 243,89 rad/s

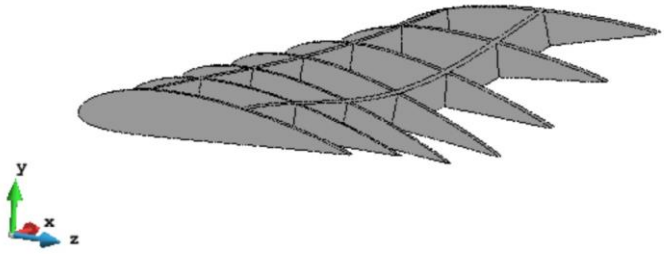

Figure 12 Mode 5: 409,90 rad/s

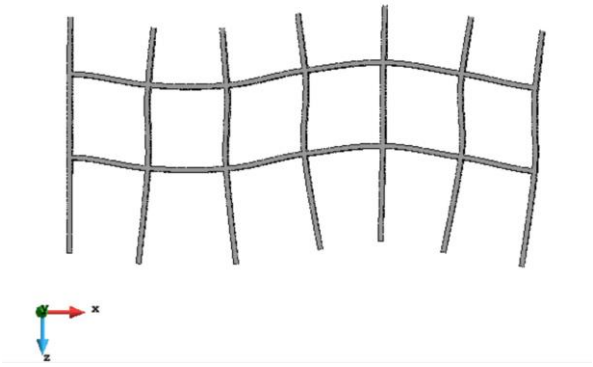

Figure 13 Mode 6: 437,23 rad/s

9. Empirical cubature method

Now that the vibrational modes for the structure have been determined, it is possible to proceed and select which set $\mathcal{Z}$ of all the Gauss integration points are the optimal integration points for the approximation of the vector of nodal internal forces $\boldsymbol{F}$. As it has been explained in *Section 6.4*, this vector of reduced internal forces can be calculated as:

$$\boldsymbol{F} \approx \sum_{g=1}^{m} \omega_g \boldsymbol{f}(\overline{\boldsymbol{x}}_g) \tag{32}$$

This set of $\mathcal{Z}$ optimal integration points are considered to be the optimal location for wing sensor placement.

The approximation of the integral of reduced vector of internal forces will be done using the Empirical Cubature Method (ECM) (Hernández et al. 2016). This project will only deal with the discrete formulation of this method, since in a FE problem the integrand is only known at specific points (integration points) rather than having a continuous representation.

Before explaining the discrete scheme, a brief presentation of the Empirical Cubature Method will be made. Let $f_I^j(\boldsymbol{x})$ denote the I^{th} component $(I = 1, 2, \dots n)$ of the integrand at point $\boldsymbol{x} \in \Omega$ corresponding to the j^{th} vibrational mode $(j = 1, 2, \dots P)$. The idea is to approximate the following integral.

$$F_I^j = \int_{\Omega} f_I^j \, d\Omega \approx \sum_{g=1}^{m} \omega_g f_I^j(\overline{\boldsymbol{x}_g}) \tag{33}$$

The set of integration points $\mathcal{Z} = \{\overline{\boldsymbol{x}}_g\}_{g=1}^{m}$ along with their associated positive weights $\boldsymbol{\omega} = [\omega_1, \omega_2, \dots, \omega_m]^T$ are selected such as the integration error falls to a minimum. The expression of the approximation error of the integral can be written as follows:

$$e_I^j = \sum_{g=1}^{m} \omega_g f_I^j(\overline{\boldsymbol{x}_g}) - \int_{\Omega} f_I^j d\Omega \tag{34}$$

The minimization problem, i.e. the set of integration points and weights such as the integration error is minimum, can be written in matrix form as:

$$(\boldsymbol{\omega}, \mathcal{Z}) = \arg \min_{\boldsymbol{\omega} \in \mathbb{R}_+^m,\ z_g \in \Omega} \|\boldsymbol{J}_{\boldsymbol{z}}\boldsymbol{\omega} - \boldsymbol{b}\|^2 \tag{35}$$

Where:

$$\boldsymbol{J}_{\mathcal{Z}} = \begin{bmatrix} \boldsymbol{f}^1(\overline{\boldsymbol{x}}_1) & \boldsymbol{f}^1(\overline{\boldsymbol{x}}_2) & \dots & \boldsymbol{f}^1(\overline{\boldsymbol{x}}_m) \\ \boldsymbol{f}^2(\overline{\boldsymbol{x}}_1) & \boldsymbol{f}^2(\overline{\boldsymbol{x}}_2) & \dots & \boldsymbol{f}^2(\overline{\boldsymbol{x}}_m) \\ \vdots & \vdots & \ddots & \vdots \\ \boldsymbol{f}^P(\overline{\boldsymbol{x}}_1) & \boldsymbol{f}^P(\overline{\boldsymbol{x}}_2) & \dots & \boldsymbol{f}^P(\overline{\boldsymbol{x}}_m) \end{bmatrix} \qquad \boldsymbol{b} = \begin{bmatrix} \int_{\Omega} \boldsymbol{f}^1\, d\Omega \\ \int_{\Omega} \boldsymbol{f}^2\, d\Omega \\ \vdots \\ \int_{\Omega} \boldsymbol{f}^P\, d\Omega \end{bmatrix} \qquad \boldsymbol{f} = \begin{bmatrix} f_1^j \\ f_2^j \\ \vdots \\ f_n^j \end{bmatrix}$$

The optimization problem posed before can become computationally laborious if the number of training configurations (vibrational modes in this case) P is very high. To solve this possible problem, the integrand f_I^j will be subjected to a dimensional reduction process. Then, the error will be calculated in terms of the orthogonal basis functions arising from this reduction.

Let us imagine that the integrand f_I^j has already been approximated via a set of $p \ll P$ basis functions obtained using some dimensionality reduction technique:

$$f_I^j(\boldsymbol{x}) \approx \sum_{i=1}^{p} \Lambda_i(\boldsymbol{x})\, c_{iI}^J \;\; (j = 1,2,\dots,P; I = 1,2,\dots,n) \tag{36}$$

As it was explained, in the SVD, Λ_i is the i^{th} basis function and c_{iI}^J is the corresponding coefficient for the approximation. Using Equation (36), the error expression can be written as:

$$e_I^j = \left(\sum_{g=1}^{m} \omega_g \Lambda_i(\overline{\boldsymbol{x}_g}) - \int_{\Omega} \Lambda_i \, d\Omega \right) c_{iI}^j \tag{37}$$

The coefficients c_{iI}^j only depend on the function being approximated and not on their position. This means that they do not play a role in the error minimization. Therefore, minimizing the error produced when approximating the integrand f_I^j is equal to minimizing the error produced in approximating the integral of the basis functions Λ_i. By using this consideration, the matrices $\boldsymbol{J_Z}$ and $\boldsymbol{b}$ are redefined to:

$$\boldsymbol{J_Z} = \begin{bmatrix} \Lambda_1(\bar{\mathbf{x}}_\mathbf{1}) & \Lambda_1(\bar{\mathbf{x}}_\mathbf{2}) & \dots & \Lambda_1(\bar{\mathbf{x}}_\mathbf{m}) \\ \Lambda_2(\bar{\mathbf{x}}_\mathbf{1}) & \Lambda_2(\bar{\mathbf{x}}_\mathbf{2}) & \dots & \Lambda_2(\bar{\mathbf{x}}_\mathbf{m}) \\ \vdots & \vdots & \ddots & \vdots \\ \Lambda_\mathrm{p}(\bar{\mathbf{x}}_\mathbf{1}) & \Lambda_\mathrm{p}(\bar{\mathbf{x}}_\mathbf{2}) & \dots & \Lambda_\mathrm{p}(\bar{\mathbf{x}}_\mathbf{m}) \end{bmatrix} \qquad \boldsymbol{b} = \begin{bmatrix} \int_\Omega \Lambda_1 \, d\Omega \\ \int_\Omega \Lambda_2 \, d\Omega \\ \vdots \\ \int_\Omega \Lambda_p \, d\Omega \end{bmatrix}$$

It can be seen how by submitting the integrand to a dimensional reduction, the rows for both matrices $\boldsymbol{J_Z}$ and $\boldsymbol{b}$ decrease from P to p ($p \ll P$). The problem of the determination of the basis functions for approximating the integrand will be dealt with in *Section 9.1.1 Basis matrices.*

9.1. Discrete formulation

The Empirical Cubature Method can be used and formulated when the integrand willing to be approximated has a continuous description. However, in a FE problem, the value of the integrand is only known at the integration points. This means that only the discrete representation of the vector of nodal internal forces $\boldsymbol{F}$ is available. In this section, the discrete formulation of the Empirical Cubature Method is presented.

As it has been explained before, the optimal integration points inside the geometry will be considered as the optimal location for the sensors of the wing. This optimal integration points arise from the approximation of the vector of nodal internal forces $\boldsymbol{F}$.

Let us keep in mind that this project is using the vibrational modes as displacement basis matrices. When calculating this vibrational modes, nor the internal nor the external forces are needed. So, how can $\boldsymbol{F}^h$ be approximated to $\boldsymbol{F}$ and then, the optimal integration points calculated if this vector is not used in the first place? Via the stress modes.

Each vibrational mode implies a deformation in the geometry. Therefore, this deformation means that internal forces arise in the structure. Considering that the problem is kept under the elastic assumptions, these stress modes that come from the deformation can be easily calculated as:

$$\boldsymbol{S} = \boldsymbol{C}\boldsymbol{\varepsilon} \tag{38}$$

Where $\boldsymbol{S}$ is the stacked stress vector

$$\boldsymbol{S} = \begin{bmatrix} \boldsymbol{\sigma}(\boldsymbol{x}_1) \\ \boldsymbol{\sigma}(\boldsymbol{x}_2) \\ \dots \\ \boldsymbol{\sigma}(\boldsymbol{x}_M) \end{bmatrix} \tag{39}$$

There will be a different stress vector $\boldsymbol{S}$ for each of the different vibrational modes.

$\boldsymbol{\varepsilon}$ is the strain vector

$$\boldsymbol{\varepsilon} = \begin{bmatrix} \boldsymbol{\varepsilon}(\boldsymbol{x}_1) \\ \boldsymbol{\varepsilon}(\boldsymbol{x}_2) \\ \dots \\ \boldsymbol{\varepsilon}(\boldsymbol{x}_M) \end{bmatrix} \tag{40}$$

It can be calculated as:

$$\boldsymbol{\varepsilon} = \boldsymbol{\mathcal{B}}^h \boldsymbol{d}^h + \boldsymbol{\mathcal{B}}_0^h \boldsymbol{d}_0^h \tag{41}$$

$\boldsymbol{\mathcal{B}}^h$ and $\boldsymbol{\mathcal{B}}_0^h$ are the stacked B matrix of unrestricted and restricted degrees of freedom respectively. $\boldsymbol{d}^h$ and $\boldsymbol{d}_0^h$ are the vector of nodal displacements of the unrestricted and restricted degrees of freedom respectively. In modal analysis (free vibration) $\boldsymbol{d}_0^h = 0$. Moreover, the nodal displacements of the unrestricted degrees of freedom $\boldsymbol{d}^h$ correspond to each one of the columns of the matrices of vibration modes. So Equation (41) can be written as:

$$\boldsymbol{\varepsilon} = \boldsymbol{\mathcal{B}}^h \boldsymbol{\Phi} \tag{42}$$

Finally, the $\boldsymbol{C}$ in Equation (38) corresponds to the stacked elasticity matrix:

$$\boldsymbol{C} = \begin{bmatrix} \boldsymbol{C}(\boldsymbol{x_1}) & \boldsymbol{0} & \boldsymbol{0} & \boldsymbol{0} \\ \boldsymbol{0} & \boldsymbol{C}(\boldsymbol{x_2}) & \boldsymbol{0} & \boldsymbol{0} \\ \boldsymbol{0} & \boldsymbol{0} & \ddots & \boldsymbol{0} \\ \boldsymbol{0} & \boldsymbol{0} & \boldsymbol{0} & \boldsymbol{C}(\boldsymbol{x_M}) \end{bmatrix} \tag{43}$$

Now that the origin of the nodal internal forces vector has been explained, the idea is now to approximate the integral of any $f_I \quad (I = 1, 2, \dots n)$ as the sum of positive, scalar weights multiplied by the function evaluated at the chosen points. (Recall that n is the number of reduced-order-model degrees of freedom and M is the number of FE integration points).

$$F_I \approx \sum_{g=1}^{M} W_g f_I\left(\overline{\boldsymbol{x}_g}\right) = \sum_{g=1}^{M} \sqrt{W_G}\left(\sqrt{W_G}\, f_I(\boldsymbol{x}_g)\right) = \sqrt{\boldsymbol{W}}^T \boldsymbol{\mathcal{F}_I} \tag{44}$$

Where $\sqrt{\boldsymbol{W}} \in \mathbb{R}^M$ is defined as the matrix of the square root of each finite element integration weight:

$$\sqrt{\boldsymbol{W}} = \left[\sqrt{W_1} \quad \sqrt{W_2} \quad \dots \quad \sqrt{W_M}\right]^T \tag{45}$$

And $\boldsymbol{\mathcal{F}_I} \in \mathbb{R}^M$ can be calculated as:

$$\boldsymbol{\mathcal{F}_I} = \begin{bmatrix} \sqrt{W_1} f_I(\boldsymbol{x}_1) \\ \sqrt{W_2} f_I(\boldsymbol{x}_2) \\ \vdots \\ \sqrt{W_M} f_I(\boldsymbol{x}_M) \end{bmatrix} \tag{46}$$

The procedure to calculate f_I is to store the components of the reduced internal forces at all integration points. To do so, the following equation is used.

$$f_I(\boldsymbol{x}_g) = \boldsymbol{\varepsilon}_I^T(\boldsymbol{x}_g)\boldsymbol{\sigma}(\boldsymbol{x}_g) \tag{47}$$

All terms of the equation have already been calculated in the project. Specifically, $\boldsymbol{\varepsilon}$ is calculated using Equation (42) and $\boldsymbol{\sigma}$ using Equation (38).

9.1.1. Basis matrices

In *Section 9 Empirical cubature method* the integrand f_I^j was approximated as $f_I^j(\boldsymbol{x}) \approx \sum_{i=1}^{p} \Lambda_i(\boldsymbol{x})\, c_{iI}^J$ to alleviate the computational power required for the optimization problem. Now, the discrete formulation of the problem is under study and, thus, the basis matrix needed to be determined are the ones for the nonlinear term $\boldsymbol{\mathcal{F}_I}$. To do so,

the procedure that will be followed is the "Expanded basis approach (EBA)" (Hernández et al. 2016; Hernández et al. 2014). From these references, it can be concluded that the basis matrix for $\boldsymbol{\mathcal{F}_I}$ is:

$$\text{EBA} = \left[\boldsymbol{\Lambda_1} \quad \boldsymbol{\Lambda_2} \quad \dots \quad \boldsymbol{\Lambda_p} \quad \sqrt{\boldsymbol{W}}\right] \tag{48}$$

To start computing $\boldsymbol{\Lambda}$, the snapshot matrix of $\boldsymbol{\mathcal{F}_I^j}$ for all components $I = 1, 2, \dots n$ and all training configurations (vibrational modes) $j = 1, 2, \dots P$ is needed.

$$\boldsymbol{\mathcal{X}_{\mathcal{F}}} = [\boldsymbol{\mathcal{F}_1^1} \quad \dots \quad \boldsymbol{\mathcal{F}_n^1} \quad \boldsymbol{\mathcal{F}_1^2} \quad \dots \quad \boldsymbol{\mathcal{F}_n^2} \quad \dots \quad \boldsymbol{\mathcal{F}_1^P} \quad \dots \quad \boldsymbol{\mathcal{F}_n^P}] \tag{49}$$

Each of the rows from the $\boldsymbol{\mathcal{X}_{\mathcal{F}}}$ matrix is calculated using the stress matrices in Equation (46), that aroused from each of the deformations modes as it was explained in *Section 9.1.* The procedure is to store the components of the reduced internal forces at all integration points and all training configurations in a snapshot matrix. A column from this matrix would look like this:

$$\mathbf{SNAP} = \begin{bmatrix} f_I(\boldsymbol{x}_1) \\ f_I(\boldsymbol{x}_2) \\ \vdots \\ f_I(\boldsymbol{x}_M) \end{bmatrix} \tag{50}$$

Likewise, the FE integration weights (including the Jacobian) have to be stored in a vector $\boldsymbol{W} \in \mathbb{R}^M$. Then,

$$\boldsymbol{\mathcal{F}_I} = \sqrt{\boldsymbol{W}} \, \mathrm{o} \, \mathbf{SNAP} = \begin{bmatrix} \sqrt{W_1} \\ \sqrt{W_2} \\ \vdots \\ \sqrt{W_M} \end{bmatrix} \mathrm{o} \begin{bmatrix} f_I(\boldsymbol{x}_1) \\ f_I(\boldsymbol{x}_2) \\ \vdots \\ f_I(\boldsymbol{x}_M) \end{bmatrix} \tag{51}$$

Next step is to compute the matrix of zero-integral snapshots $\widehat{\boldsymbol{\mathcal{X}}}_{\mathcal{F}}$

$$\widehat{\boldsymbol{\mathcal{X}}}_{\mathcal{F}} = [\widehat{\boldsymbol{\mathcal{F}}}_1^1 \quad \dots \quad \widehat{\boldsymbol{\mathcal{F}}}_n^1 \quad \widehat{\boldsymbol{\mathcal{F}}}_1^2 \quad \dots \quad \widehat{\boldsymbol{\mathcal{F}}}_n^2 \quad \dots \quad \widehat{\boldsymbol{\mathcal{F}}}_1^P \quad \dots \quad \widehat{\boldsymbol{\mathcal{F}}}_n^P] \tag{52}$$

This matrix can be easily computed by applying the following formula to each column of $\boldsymbol{\mathcal{X}}_{\mathcal{F}}$.

$$\widehat{\boldsymbol{\mathcal{F}}}_I^j = \boldsymbol{\mathcal{F}}_I^j - \frac{\sqrt{\boldsymbol{W}}}{\|\sqrt{\boldsymbol{W}}\|}\left(\frac{\sqrt{\boldsymbol{W}}^T}{\|\sqrt{\boldsymbol{W}}\|}\boldsymbol{\mathcal{F}}_I^j\right) \tag{53}$$

Finally, the matrix of orthogonal basis functions $\boldsymbol{\Lambda}$ can be calculated applying a SVD of rank p to the matrix $\widehat{\boldsymbol{\mathcal{X}}}_{\mathcal{F}}$, i.e.:

$$\widehat{\boldsymbol{\mathcal{X}}}_{\mathcal{F}} \approx \boldsymbol{\Lambda}\boldsymbol{\Sigma}_{\Lambda}\boldsymbol{V}_{\Lambda}^T \tag{54}$$

Where $\boldsymbol{\Sigma}_{\Lambda}$ and $\boldsymbol{V}_{\Lambda}^T$ are the matrices of singular values and right singular vectors respectively, associated to the selected dominant left singular vectors $\boldsymbol{\Lambda}$.

9.1.2. Minimization problem

Now that the matrix of singular vectors has been computed, next step is to determine the optimal location of integration points using the minimization error formula seen in Equation (35) but written for the discrete case.

$$(\boldsymbol{\alpha}, \boldsymbol{\mathcal{Z}}) = \arg\min_{\boldsymbol{\alpha}\geq\boldsymbol{0},\boldsymbol{z}} \|\boldsymbol{J}_{\boldsymbol{z}}\boldsymbol{\omega} - \boldsymbol{b}\|^2 \tag{55}$$

Matrices $\boldsymbol{J}_{\boldsymbol{z}} \in \mathbb{R}^{p+1xm}$ and $\boldsymbol{b} \in \mathbb{R}^{p+1}$ can be calculated as:

$$\boldsymbol{J}_{\boldsymbol{z}} = \left[\boldsymbol{\Lambda}_{\mathcal{Z}} \quad \sqrt{\boldsymbol{W}}_{\mathcal{Z}}\right]^T; \qquad \boldsymbol{b} = [\boldsymbol{0}^T \quad V]^T \tag{56}$$

Where $V = \int_{\Omega} d\Omega$ is the volume of the domain.

Once the problem in Equation (55) is solved, the set of integration points $\mathcal{Z}$ is found among all the possible Gauss points of the mesh and their corresponding weights can be calculated as:

$$\omega_g = \sqrt{W_g}\alpha_g, \quad g = 1, 2, \dots, m \tag{57}$$

9.2. Obtaining the sensor location

Once all the previous steps are followed, the set of $\mathcal{Z}$ integration points and their relative weights is obtained by the algorithm proposed in (Hernández, et al. 2016). Figure 14 shows the outline of the location of these elements selected.

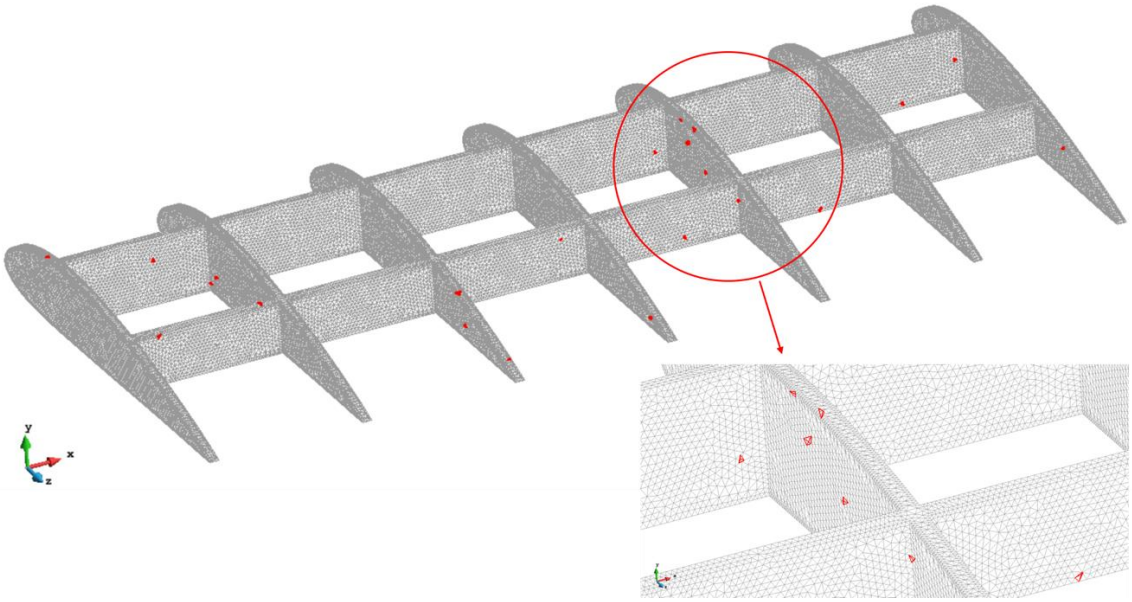

Figure 14 Location of the set of optimal integration points (in red)

Because of the reasons explained in *Section 6.5 Sensor location,* these selected points can be considered as the optimal location for wing sensors.

9.2.1. Convergence to the absolute minimum

Recall that the set of integration points $\mathcal{Z}$ were determined in a way such as the integration error fell to a minimum (absolute zero). To check if the previously selected points meet this requirement, Figure 15 is plotted. In this figure, the dimensionless residual $\|\boldsymbol{r}\|/\|\boldsymbol{b}\| = \|\boldsymbol{r}\|/V$ versus the number of points m is shown.

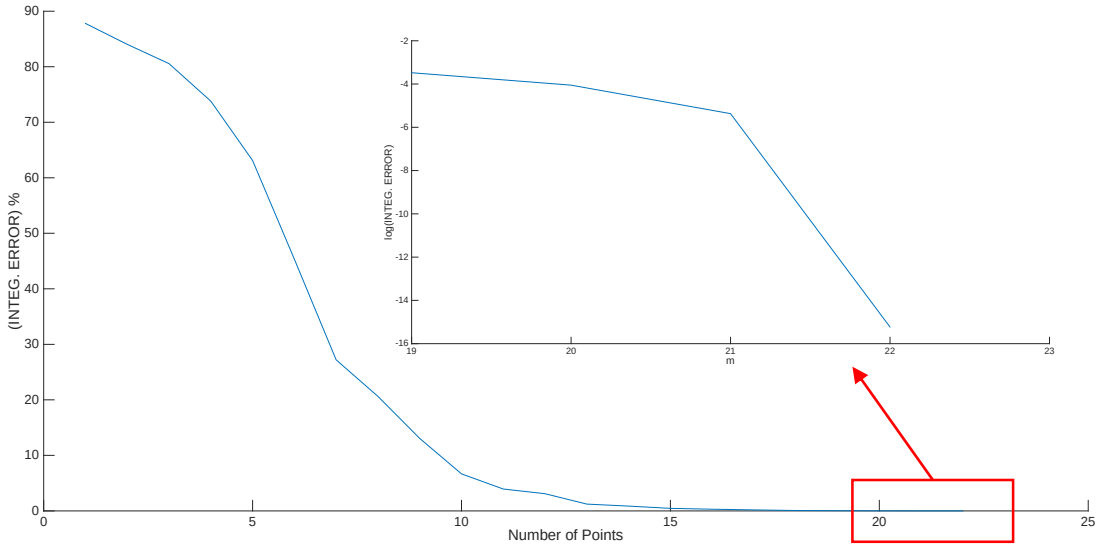

Figure 15 Dimensionless residual ||r||/||b||= ||r||/V versus the number of points m

It can be seen how, as the number of integration points m increases, the integration error decreases until it falls to a negligible value (~ 10^{-15}) when $m = 22$. In (Hernández, Caicedo y Ferrer 2016) it is stated that the error using algorithm for the greedy selection method converges to zero when the number of selected points $m = p + 1$. In the case of this project, $p = number\ of\ deformation\ modes\ x\ number\ of\ stress\ modes = 6\ x\ 6 = 36$. So m should be at maximum 37. Nevertheless, less integration points could be required.

It turns out that integrating exactly 6 modes requires 21 points (+ 1 for the volume). Notice that this figure coincides with the number of independent components of the $n \times n$ reduced stiffness matrix (plus 1).

The reduced stiffness matrix $\boldsymbol{K} \in \mathbb{R}^{nxn}$ can be calculated by pre-multiplying and post-multiplying the FE stiffness matrix by the matrix of modes $\boldsymbol{\Phi} \in \mathbb{R}^{Nxn}$.

$$\boldsymbol{K} = \boldsymbol{\Phi}^T \boldsymbol{K}^h \boldsymbol{\Phi} \tag{58}$$

In the case concerning this project, $n = 6$. Hence, matrix $\boldsymbol{K}$ has $6x6 = 36$ components. However, matrix $\boldsymbol{K}$ is symmetrical, i.e. only 21 of these components are independent.

10. Results validation

Now that the methodology for locating the optimal integration points inside the mesh has been determined, and thus the location of the sensors in order to detect the vibrational modes of the structure, it is time to check if the results obtained are correct. The test is simple: the vibrational modes and frequencies obtained have to be the same when calculating them using the full-order model (FE analysis) or the ROM.

To do so, the construction of the Reduced-Order Model is needed.

10.1. Reduced-order model reconstruction

To obtain the vibrational modes and frequencies the same equation as in the FE analysis needs to be solved.

$$\boldsymbol{M}^h \ddot{\boldsymbol{d}}^h + \boldsymbol{K}^h \boldsymbol{d}^h = \boldsymbol{0} \tag{59}$$

However, the construction of the ROM will take advantage of the optimal integration points and weights obtained in the previous sections. This means that the previous equation changes all its terms to the reduced-order counterparts.

$$\boldsymbol{M}\ \ddot{\boldsymbol{d}} + \boldsymbol{K}\ \boldsymbol{d} = \boldsymbol{0} \tag{60}$$

The two matrices needed to compute the natural frequencies and the vibrational modes are the reduced mass matrix $\boldsymbol{M}$ and the reduced stiffness matrix $\boldsymbol{K}$.

10.1.1. Reduced stiffness matrix

The reduced stiffness matrix $\boldsymbol{K}$ can be calculated following two different procedures:

1. Pre-multiplying and post-multiplying the FE stiffness matrix by the modes matrices as seen in Equation (61).

$$\boldsymbol{K} = \boldsymbol{\Phi}^T \boldsymbol{K}^h \boldsymbol{\Phi} \tag{61}$$

   Remember that $\boldsymbol{K}$ and $\boldsymbol{K}^h$ denote the reduced-order and full-order stiffness matrix respectively. $\boldsymbol{\Phi}$ denotes the matrix of the different vibrational modes.

2. Calculate the ROM stiffness matrix only at the optimal integration points. This is the procedure that will be followed since will show how the integration points selected are able to correctly reconstruct the vibrational modes calculated using the full-order model.

10.1.1.1. ROM STIFFNESS MATRIX CALCULATION

As it has been explained in *Section 9 Empirical cubature method*, the Empirical Cubature Method (ECM) obtains a set of integration points and weights such as the integration error is minimized. Using these points and weights, the reduced stiffness matrix $\boldsymbol{K} \in \mathbb{R}^{PxP}$ can be calculated as:

$$\boldsymbol{K} = \sum_{g=1}^{m} \boldsymbol{K}(\mathcal{Z}_g)\omega_g \tag{62}$$

Where $\mathcal{Z}$ is the set of m Gauss points selected using the ECM and ω are their respective weights. $\boldsymbol{K}(\mathcal{Z}_g)$ is the elemental stiffness matrix of the Finite Element that contains the Gauss point evaluated in the Gauss point $\mathcal{Z}_g$ pre-multiplied by the entries of the vector

of modes that correspond to the degrees of freedom of that element, transposed, and post-multiplied by the same vector of modes.

$$\boldsymbol{K}(\mathcal{Z}_g) = \boldsymbol{\Phi}^{eT}\boldsymbol{K}^{\boldsymbol{e}}\boldsymbol{\Phi}^{e} \tag{63}$$

As opposed to the calculation of $\boldsymbol{K}^{h}$ where polynomial basis element by element were used, in the calculation of its ROM counterpart, global basis are used and the Gauss integration method is no longer necessary. Now the integration is adapted to each problem vie the Empirical Cubature Method.

10.1.2. Reduced mass matrix

The procedure to calculate the reduced mass matrix is the same as the one followed for the stiffness matrix.

$$\boldsymbol{M} = \sum_{g=1}^{m} \boldsymbol{M}(\mathcal{Z}_g)\omega_g \tag{64}$$

And $\boldsymbol{M}(\mathcal{Z}_g)$ can be calculated as

$$\boldsymbol{M}(\mathcal{Z}_g) = \boldsymbol{\Phi}^{eT}\boldsymbol{M}^{\boldsymbol{e}}\boldsymbol{\Phi}^{e} \tag{65}$$

10.2. Comparison between FEM and ROM

Once the reduced mass and stiffness matrices are calculated, the natural frequencies using the ROM can be computed. Table 3 shows the values of the frequencies obtained for both, the analysis using the FE method and the ROM as well as their approximated computing time.

	Natural frequencies (rad/s)	
Method (Elements)	Full-order (550.000)	Reduced-order (22)
Mode 1	73,01	73,01
Mode 2	77,85	77,85
Mode 3	127,56	127,56
Mode 4	243,89	243,89
Mode 5	409,90	409,90
Mode 6	437,23	437,23
Computing time	3' 32"	16”

Table 3 FEM vs ROM natural frequencies comparison

As it can be seen in Table 3, the results obtained using the ROM are exactly the same as the ones obtained by computing the full order model. A substantial reduction in the computing time can be appreciated between the two methods. More precisely, the ROM computing time is 13,25 times lower than its FEM counterpart.

11. Practical application

Now that the methodology for locating the optimal integration points inside the mesh has been determined, and thus the location of the sensors in order to detect the vibrational modes of the structure, this second part of the project will show the real potential of the Empirical Cubature Method in computational problems.

This section of the project will compute a ROM, using the same methodology employed in the previous section, capable of calculating, almost immediately, the natural frequencies and vibrational modes of the geometry under study when a part or parts of the structure have changed its elastic properties (Young's modulus) due to, for example, a partial crack. Of course, the results obtained will be based in a reduced model. Hence they will be an approximation.

11.1. Problem description

Imagine that using some experimental methodology, it has been detected that the Young's modulus of the structure at points 1, 2 and 3 shown in Figure 16 has decreased by a factor of 'A', 'B' and 'C' respectively.

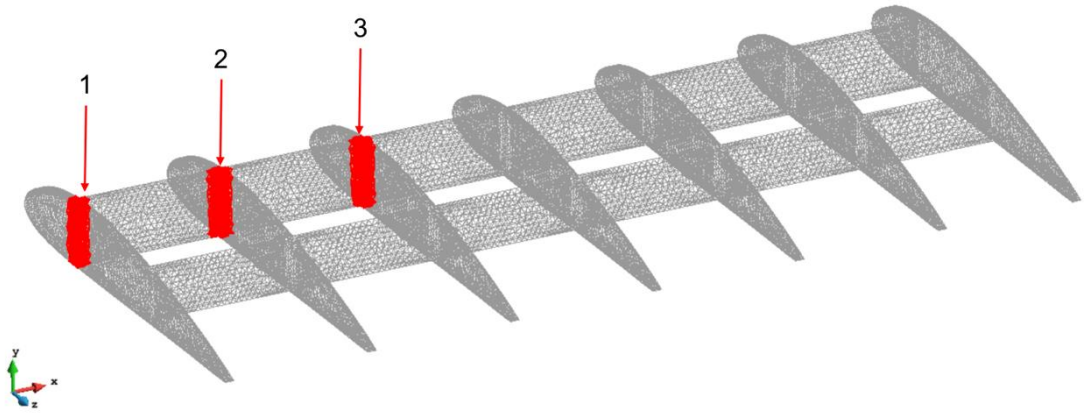

Figure 16 Damaged elements

In order to now compute the natural frequencies, a full FE analysis would be needed. Let's assume that the mass matrix $\boldsymbol{M}^h$ remains constant and thus it only needs to be calculated once and then it can be used for every different configuration under study.

Right now the stiffness matrix $\boldsymbol{K}^h$ has to be calculated (and is different for every configuration) by discretizing the geometry in N different elements (in the case of this project 550.000) and calculate the elemental contribution $\boldsymbol{K}^e$ of each element to the global matrix $\boldsymbol{K}^h$ by means of Gauss integration using a 4-Gauss-point rule. That means calculating $M = 4N$ Gauss points in total. This operation is very time and computing-demanding. Moreover, if the results are expected almost immediately, the only way to meet this requirement, if solving the full-order FE problem, is to precompute $\boldsymbol{K}^h$ for all combinations of different factors A, B and C ranging between two plausible different values and store them in memory so the stiffness matrix does not need to be assembled. This methodology is not feasible.

11.2. Proposed solution

As it has been explained before, since the mass matrix $\boldsymbol{M}^h$ remains constant it only needs to be calculated once. It is clear then, that the bottleneck that avoids the calculation of natural frequencies to be immediate is having to compute the stiffness matrix $\boldsymbol{K}^h$. To solve this problem a reduced order model will be used, where the stiffness matrix is going to be calculated by means of the integration points and weights obtained via ECM.

11.2.1. Basis matrix calculation

The idea of model reduction relies on the premise that any vector or matrix in the problem statement can be projected onto the reduced order space using the matrix of basis vectors $\boldsymbol{\Phi} \in \mathbb{R}^{Nxn}$. There are various procedures for computing the basis matrix

Φ. The most common one and the one that will be used in this project is to, first, solve the full-order problem (FE problem) for representative values of input parameters $\boldsymbol{\mu}$. Then, collect the corresponding results obtained in a snapshot matrix.

$$\boldsymbol{X}_d = [\boldsymbol{d}^h(\boldsymbol{\mu}^1) \quad \boldsymbol{d}^h(\boldsymbol{\mu}^2) \quad \dots \quad \boldsymbol{d}^h(\boldsymbol{\mu}^P)] \tag{66}$$

In the case of this project, the input parameters are the different factors 'A', 'B' and 'C' that the Young's modulus of the structure has decreased at the previously shown points. The different results obtained correspond to the P vibrational modes calculated for each configuration K. So the snapshot matrix will look like this:

$$\boldsymbol{X}_d = \left[\boldsymbol{d}^h(\boldsymbol{\mu}^1)^1 \quad \boldsymbol{d}^h(\boldsymbol{\mu}^1)^2 \quad \dots \quad \boldsymbol{d}^h(\boldsymbol{\mu}^1)^P \quad \boldsymbol{d}^h(\boldsymbol{\mu}^2)^1 \quad \dots \quad \boldsymbol{d}^h(\boldsymbol{\mu}^K)^P\right] \tag{67}$$

It has been considered that the Young's modulus of the structure at these points will only vary between the values $E_{min} = \frac{E}{100}$ and $E_{max} = E$. Three different samples of the interval have been used to calculate the snapshot matrix. This means that each point has three possible Young's modulus ($E_1 = \frac{E}{100}, E_2 = \frac{E}{50}, E_3 = E$).

These different calculations using the different parameters are called the training configurations. These configurations are what the ROM uses to approximate the solution. This means that the more configurations are trained into the model, the more precise the approximations will be. In this project, 5 different training configurations were used ($K = 5$). Each configuration has $P = 6$ different displacement vectors or vibrational modes. This means matrix $\boldsymbol{X}_d \in \mathbb{R}^{KPxN}$. In Table 4, the different configurations are schematized.

Training configuration	E_1	E_2	E_3
1	E	E	E
2	$\frac{E}{50}$	$\frac{E}{50}$	$\frac{E}{50}$
3	$\frac{E}{100}$	$\frac{E}{100}$	$\frac{E}{100}$
4	$\frac{E}{100}$	$\frac{E}{50}$	E
5	$\frac{E}{50}$	$\frac{E}{100}$	E

Table 4 Training configurations

As it can be seen, the dimensions of the matrix $\boldsymbol{X}_d$ depend greatly on the number of elements N in the mesh. In order to reduce the computational burden this supposes, and to be able to solve the problem with an average computer, a mesh of $N = 100.000$ elements is used (instead of the one of 550.000 elements used in the first section of the project). This means that the results obtained concerning the natural frequencies will not be as accurate as the ones obtained using the mesh with 550.000 elements. However, the methodology used can be extrapolated if a more powerful computer is available.

The following table shows the comparison between the natural frequencies of the structure when the factors A, B and C are all 1 (the structure suffers from no damage) and when all these factors are 100 (most critical situation studied).

		Natural frequencies (rad/s)					
		MODE 1	**MODE 2**	**MODE 3**	**MODE 4**	**MODE 5**	**MODE 6**
Factors of reduction	**A, B, C = 1**	74,13	89,28	145,75	280,85	430,30	506,46
	A, B, C = 100	46,67	62,38	122,01	229,84	292,90	425,80

Table 5 Natural frequency comparison between the normal configuration and the most damaged configuration

As it can be seen in Table 5, the natural frequencies vary substantially with the damaged elements. In a real-life scenario, it would be important to monitor the health of the structure in order to detect these changes and prevent the structure from resonating.

Once the snapshot matrix of displacement is calculated, the same steps as the ones followed during the first part of the project have to be followed until the final determination of the new set of integration points and their respective weights.

1. Calculate the stress modes. This step is specially tricky since the internal forces for each configuration are computed using as an input all the deformation modes in matrix $\boldsymbol{X}_d$. Recall that now the elasticity matrix for each configuration changes, i.e. each set of stress modes need to be computed using their respective elasticity matrix.
2. Store the components of the reduced internal forces at all integration points and all training configurations in the snapshot matrix $\boldsymbol{X}_{\mathcal{F}}$
3. Compute the matrix of zero-integral snapshots $\widehat{\boldsymbol{X}}_{\mathcal{F}}$
4. Determine an orthogonal basis matrix $\boldsymbol{\Lambda}$
5. Construct the matrices $\boldsymbol{J}$ *and* $\boldsymbol{b}$ as $\boldsymbol{J} = [\boldsymbol{\Lambda} \quad \sqrt{\boldsymbol{W}}]^T$ and as $\boldsymbol{b} = [\boldsymbol{0}^T \quad V]^T$
6. Determine the set of integration points $\mathcal{Z} \in \mathbb{N}^m$ and their associated weights $\boldsymbol{\omega} \in \mathbb{R}_+^m$ by means of the greedy selection method. In the case that is being dealt with, 1551 integration points are necessary (out of the approximately 400.000 integration points). Figure 17 shows the location of these points in the mesh.

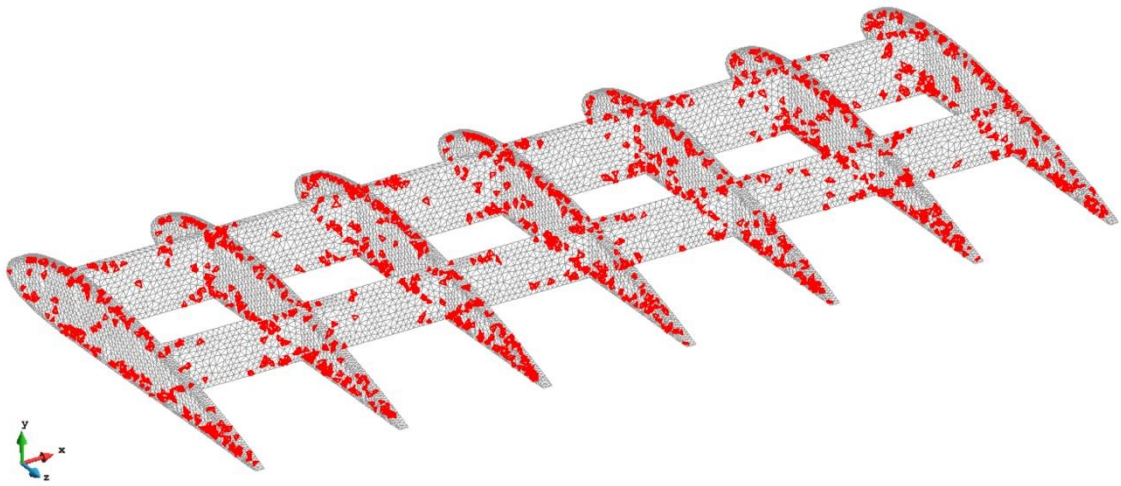

Figure 17 Location of the set of optimal integration points

In Figure 18 it can be seen how the integration error falls to zero when $m = 1551$ integration points.

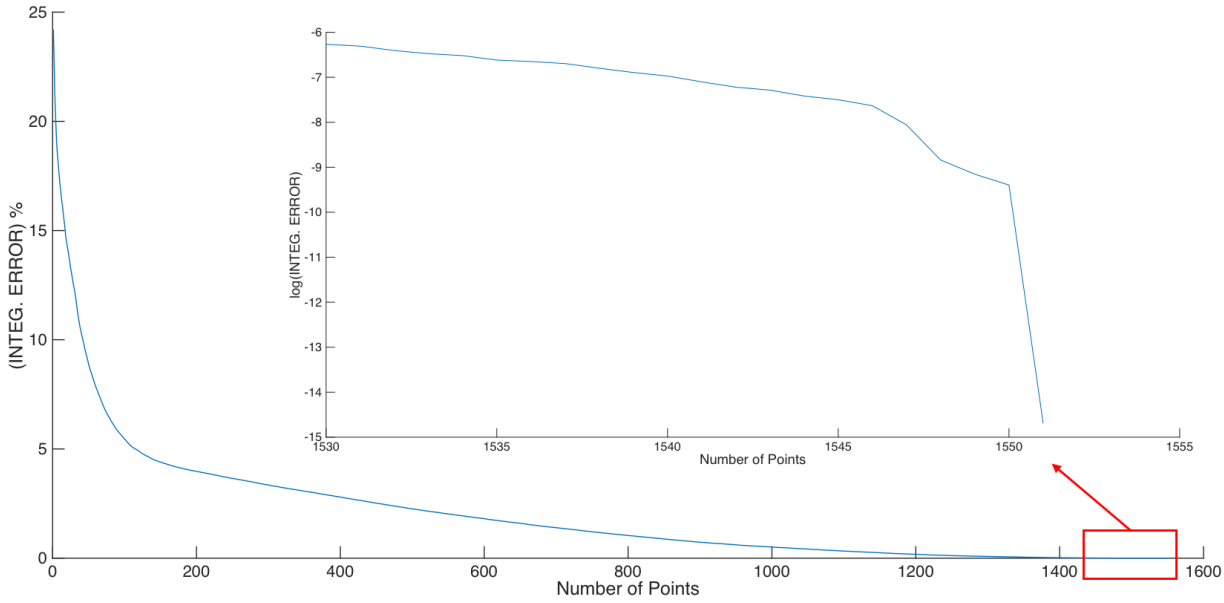

Figure 18 Dimensionless residual ||r||/||b||= ||r||/V versus the number of points m

11.2.2. Reduced mass and stiffness matrices

The objective of this second part of the project was to construct a ROM capable of calculating the natural frequencies and vibrational modes of the geometry under study almost immediately, when some part or parts of the structure have varied its elastic properties.

Now that the optimal integration points and their associated weights for the different training configurations have been calculated, it is possible to build the reduced-order model. The two matrices needed to compute the natural frequencies and the vibrational modes are the reduced mass matrix $\boldsymbol{M}$ and the reduced stiffness matrix $\boldsymbol{K}$.

11.2.2.1. Reduced mass matrix

As stated in the problem description, the structure suffers from a change in the elastic properties. However, the mass distribution along the geometry is considered to remain constant. For this reason, the reduced mass matrix $\boldsymbol{M}$ only needs to be calculated once and the calculations are quite straightforward. The full-order mass matrix $\boldsymbol{M}^h$ needs to be projected onto the reduced-order space by means of the matrices of vector modes.

$$\boldsymbol{M} = \boldsymbol{\Phi}^T \boldsymbol{M}^h \boldsymbol{\Phi} \tag{68}$$

Since this matrix only needs to be calculated once, having to compute the full-order matrix to obtain its reduced counterpart is not troubling. The matrix $\boldsymbol{M}^h$ can be stored when the different training configurations are being calculated. Then, when the matrix of vector modes is completed, $\boldsymbol{M}$ can be easily calculated and stored. Another procedure to compute $\boldsymbol{M}$ would be to follow the explanations given in *Section 10.1.2.*

11.2.2.2. Reduced stiffness matrix

The assembly of the reduced stiffness matrix has already been explained in *Section 10.1.1.*

11.3. First numerical validation

Now that the reduced mass and stiffness matrices have been calculated, it is time to validate the results obtained. The first validation will compare the results obtained in the natural-frequencies calculation between the full-order model and ROM when the Young's modulus reduction in the three points of the structure coincides with one of the training configurations.

The configuration chosen for the first numerical validation corresponds to the following reductions in the Young's modulus.

$$E_1 = \frac{E}{100} \; ; \; E_2 = \frac{E}{50} \; ; \; E_3 = E$$

The natural frequencies obtained using both the FE method and the ROM can be seen in Table 6. As well as the frequencies, the required computation time for each configuration is shown.

	Full-order	**Hyper-reduced**
MODE 1	49,84	49,84
MODE 2	73,06	73,06
MODE 3	128,09	128,09
MODE 4	246,66	246,66
MODE 5	377,80	377,80
MODE 6	461,52	461,52
Computing time	50"	4"

Table 6 Natural frequencies of a training configuration calculated using the full-order model and the ROM

It can be seen how the results obtained using both methods are exactly the same. It is important to highlight how the computing time is drastically decreased. This reduction in time would be even more striking if the 550.000-element mesh was used.

Of course, the representation of the vibrational modes is also perfectly reconstructed. Figure 19 and Figure 20 show the deformation produced by the vibrational mode number 4 when calculated using the full-order FE analysis and the ROM respectively. It can be seen how the results obtained are exactly the same.

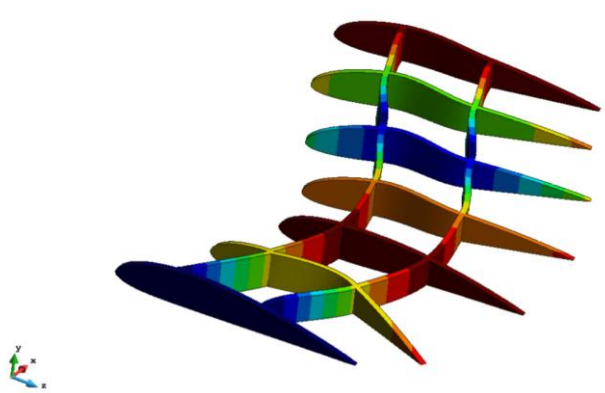

Figure 19 Mode 4 calculated using full FE analysis[2]

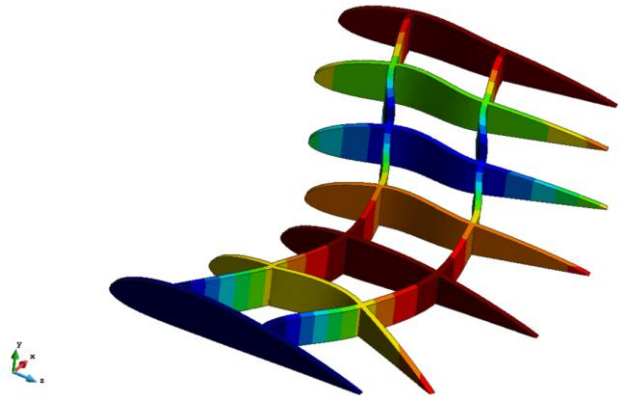

Figure 20 Mode 4 calculated using ROM

This numerical validation could be performed for every training configuration and vibrational mode and the results obtained using the Hyper-reduced model would be the same as the ones in the full-order model. This means that the ROM can perfectly reproduce the configurations it has been trained for.

[2] The color code that appears in the deformation modes is only used to designate areas with the same deformation. However, these deformations do not have a specific value (these are only deformation modes). For this reason, there is no color legend.

11.4. Second numerical validation

With the first numerical validation it can be seen how the reduced-order model can perfectly reproduce the results for which it has been trained. However, this is not the real potential of this methodology. The objective was to accurately approximate the results when the geometry suffered from a variation of the elastic properties within the previously established interval. And thanks to this methodology this can be accomplished almost immediately.

Now let's assume that via some measuring device, the elastic properties of the material in the three points of study have been determined and the results are:

$$E_1 = \frac{E}{70} \; ; \; E_2 = \frac{E}{40} \; ; \; E_3 = \frac{E}{20}$$

This configuration was not supposed in the training of the ROM. Nevertheless, the model can still be used and the results approximated using the integration points and weights previously calculated. This same configuration has been studied using the full-order model to check if the results obtained using the ROM were accurate enough. In Table 7, the results for both the ROM and full-order model are shown, as well as the computation time required and the relative error in the approximation of the ROM.

	Full-order	**Hyper-reduced**	**Error**
MODE 1	50,91	50,92	0,01%
MODE 2	68,09	68,13	0,05%
MODE 3	127,45	127,48	0,02%
MODE 4	242,48	242,52	0,02%
MODE 5	353,85	353,97	0,03%
MODE 6	442,57	442,76	0,04%
Computing time	47"	3,9"	

Table 7 Natural frequencies of a new configuration calculated using the full-order model and the ROM

Note how, even though the configuration was not trained when calculating the reduced-order model, the results obtained are very accurate and the computation time has been reduced by a factor of 12.

Figure 22 and Figure 23 show the second vibrational mode when calculating it using the full-order FE analysis and the ROM respectively. It can be seen how the error committed computing the ROM is too small to be visible in the vibrational modes. The same results would be obtained with the other vibrational modes.

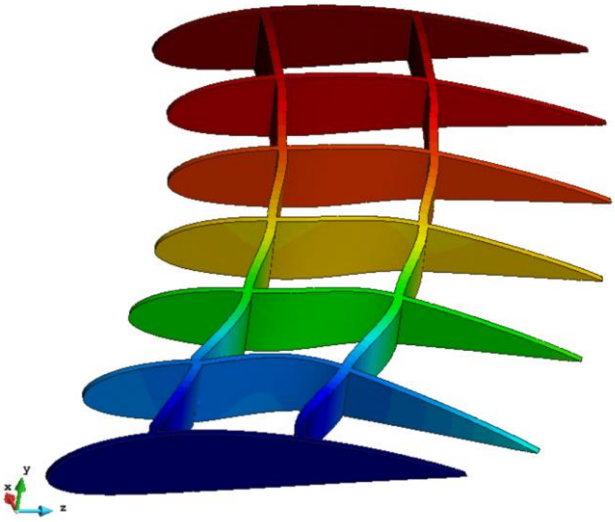

Figure 21 Second mode calculated using full FE analysis

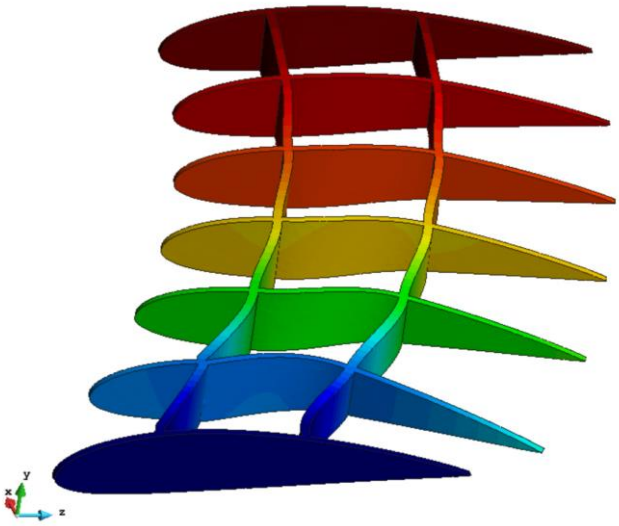

Figure 22 Second mode calculated using the ROM

12. Organization, planning and scheduling

12.1. Work breakdown structure

This section includes the planning of this project. This was done before starting the project in order to develop it as efficiently as possible. First, the project was divided in different parts according to the different steps of the project. Then, some of this parts were subdivided into tasks.

Once the tasks had been defined, the interdependencies among them were set. This step was important in order to see which tasks were independent and could be begun at any time of the project, and which of them were dependent from others and, thus, had to wait until the previous tasks had finished.

This project turned out to be very linear and the three big blocks of tasks (FE analysis, optimal integration point selection and ROM formulation) came one right after the other and the following tasks could not have started until the previous ones were completed. Moreover, since the project was completed individually, parallelization of tasks was not possible.

The organization and planning followed for the development of the project tried to respect the initial task description and calendar proposed in the Project Charter. However, as the project advanced, some of the tasks turned out to be more complicated than expected and several problems arouse.

Yet, the initial organization devised finishing the project approximately two weeks before due date in order to be able to calmly deal with possible delays.

12.2. Future work

In this section the future tasks that need to be done to improve the results of this study are described. The aim of this is not to give a detailed schedule of the following tasks but to give a brief description of the improvements that can be applied to the code.

- **Develop FE Code considering shell elements:** as it was explained in *Section 7.2* the best finite element to discretize the domain due to being made of flat plates is the shell element. However, implementing a code contemplating this type of element can be considered a project itself. This would be a good follow-up work to this project. It would allow to compare the vibrational frequencies obtained. More importantly, it would be interesting to see in how many shell elements does the geometry need to be discretized in order to obtain the same (or approximately the same) results. Then, compare the computational time.

- **Improve geometry under study:** since the main goal of this project was not to find exact results, but to present an innovative and impressive methodology to build a ROM capable of obtaining exact results almost immediately, the geometry under study was fairly simplified and differs quite a lot from a real wing. To obtain more accurate results on the vibrational modes of a wing, the geometry needs to be perfected.

  Moreover, the geometry has been considered isotropic. Nowadays most aeronautical structures are made out of composites. Introducing this fact to the study would change the values of the results obtained. However, the methodology followed to build the ROM would remain the same.

- **Improve discretization:** during the present study, the 550.000-element discretization was considered accurate enough. The reasons for this assumption are the same stated in the previous point as well as for the fact that an average computer can barely handle the huge matrices that arise from the FE analysis of

a 550.000-element mesh. However, the mesh could be refined using a cluster. Then more accurate results would be obtained.

- **Improve efficiency of code:** improving the efficiency of the code could reduce the computation time for both, the FE analysis and the ROM.

- **Build a prototype:** the study of sensor location has been carried out theoretically. Building a prototype and placing the sensors in the calculated locations to try and obtain the vibrational modes and frequencies would corroborate if these theoretical locations can be used practically or are only eligible for building the ROM.

13. Conclusions and recommendations

The objective of the present project was to determine the optimal location for wing sensors using model-order reduction for predicting the vibration behavior of a wing. The methodology to achieve this goal was to construct, using as starting point finite element simulations, a reduced-order model able to capture the essential vibrational characteristic of the wing. The basic requirements were that the code had to be programmed using the commercial software Matlab and that the ROM would be constructed following the projection-based method "Proper Orthogonal Decomposition (POD)".

To face the huge challenge that this project supposed, the precise tasks that were going to be developed were identified, including a brief description.

Not only was this project a challenge because of its magnitude, but also because, even though it is based in content explained during the degree, most of the concepts regarding model-order reduction were new to the author. For this reason, a lot of literature review on the subject was necessary as well as proposing a clear problem approach.

Once the previously-unknown concepts began to be clear, it was time to sketch a wing structure to study it, using the commercial software "SolidWorks". The final design is a simplified version of a typical rectangular wing, where all the structural elements such as spars and stingers have been represented as a pair of long beams crossing all foils.

In order to perform the finite-element analysis and obtain the vibrational modes, the geometry had to be meshed. This step was done with the help of the preprocessing engine of the software GiD. The final mesh is made out of approximately 550.000 tetrahedral elements.

Once the six first vibrational modes and their respective frequencies were calculated and plotted using the post processing engine at GiD, the Empirical Cubature Method was used to determine a set of 22 optimal integration points and weights. These points are particular because with only these 22 integration points it is possible to reconstruct, without falling into any integration error, the vibrational modes of the wing, when in the full-order FE analysis 2.200.000 integration points were needed (4 for each of the 550.000 elements).

For this reason, the location of wing sensors was considered as the location in the geometry of the optimal integration points, due to their property of correctly reconstructing the vibrational state of the structure even though the information is only available at certain points (just as in physical sensors).

Finally, it is important to highlight the drastic reduction in both computing time and memory needed when calculating the reduced-order model compared to the full-order finite element analysis. The stiffness matrix and mass matrix see their dimensions reduced from a square sparse 360.843 by 360.843-element matrix to a 6 by 6 matrix. For this reason, the assembly of both matrices and the calculation of the vibrational modes can be computed much faster. Specifically, 13,25 times faster.

Once the methodology regarding the selection of the optimal integration points was clear, a second section of the project begun, where a more practical approach was given to the hyper-reduced model.

In this second section, it was supposed that it had been detected that the Young's modulus of the structure at some selected points had decreased by a specific factor. Then, using a reduced order model created by computing different training configurations for the wing, the new vibration frequencies could be approximated committing almost zero error and making the process 12 times faster than with the full-order finite element analysis.

This decrease of the necessary computing time while maintaining good quality results is what makes reduced-order models appealing and necessary for any technological industry wanting to improve their products.

Historically, the finite-element method introduced multiple advances in aircraft design. Nowadays traditional numerical simulations are obsolete due to the complexity of the problems willing to be solved and reduced-order models are appearing to alleviate these computational burdens. There is still a long of path to cover, but it will definitely be worth keeping an eye on the advancements in this field that will help the aerospace industry, among others, simulate and design more efficient and innovative geometries and materials.

14. Bibliography

AN, S.S., KIM, T. y JAMES, D.L., 2008. Optimizing cubature for efficient integration of subspace deformations. *ACM Transactions on Graphics*, vol. 27, no. 5, pp. 1. ISSN 07300301. DOI 10.1145/1409060.1409118.

ALLAIRE, D., KORDONOWY, D., LECERF, M. et al., 2014. Multifidelity DDDAS methods with application to a self-aware aerospace vehicle. *Procedia Computer Science,* vol 29. ISSN 18770509. DOI 10.1016/j.procs.2014.05.106

ARCOS, R., 2015. Vibracions mecàniques. . S.l.: s.n.,

CHATTERJEE, A., 2000. An introduction to the proper orthogonal decomposition. [en línea]. [Consulta: 26 enero 2016]. Disponible en: http://www.iith.ac.in/~ashok/Maths_Lectures/Tutorial/tutorial2.pdf.

GHOREYSHI, M., YOUNG, M.E., LOFTHOUSE, A.J., JIRÁSEK, A. y CUMMINGS, R.M., 2016. Numerical Simulation and Reduced-Order Aerodynamic Modeling of a Lambda Wing Configuration. *Journal of Aircraft* [en línea], pp. 1-22. ISSN 0021-8669. DOI 10.2514/1.C033776. Disponible en: http://arc.aiaa.org/doi/10.2514/1.C033776.

HERNÁNDEZ, J.A., 2015. *Chapter 4 CLASSICAL LINEAR ELASTODYNAMICS*. S.l.: s.n.

HERNÁNDEZ, J.A., CAICEDO, M.A. y FERRER, A., 2016. Dimensional hyper-reduction of parameterized , nonlinear finite element models via empirical cubature. ,

HERNÁNDEZ, J.A., OLIVER, J., HUESPE, A.E., CAICEDO, M.A. y CANTE, J.C., 2014. High-performance model reduction techniques in computational multiscale homogenization. *Computer Methods in Applied Mechanics and Engineering*, vol. 276, pp. 149-189. ISSN 00457825. DOI 10.1016/j.cma.2014.03.011.

HUGHES, T., 1987. *The finite element method: linear static and dynamic finite element analysis*. S.l.: s.n. ISBN 013317025X,9780133170252.

KIM, T. y JAMES, D.L., 2011. Physics-based Character Skinning using Multi-Domain Subspace Deformations. *Proc. of ACM SIGGRAPH/Eurographics Symposium on Computer Animation 2011* [en línea], pp. 63-72. DOI 10.1145/2019406.2019415. Disponible en: http://www.cs.cornell.edu/projects/FST/.

LIEU, T., FARHAT, C. y LESOINNE, M., 2006. Reduced-order fluid/structure modeling of a complete aircraft configuration. *Computer Methods in Applied Mechanics and Engineering*, vol. 195, no. 41-43, pp. 5730-5742. ISSN 00457825. DOI 10.1016/j.cma.2005.08.026.